The East Greenland Current

Structure and Variability

Cand. Scient. Thesis
in
Physical Oceanography

Frank Gaardsted
Geophysical Institute, University of Bergen
UNIS, University Centre on Svalbard
December 2004

UNIS

Acknowledgements

First of all I would like to thank my supervisors, Tor Gammelsrød and Svein Østerhus, for the possibility of working with a very interesting subject, and for the support and helpful discussions. I would also like to thank Frank Nilsen for making the stay at UNIS possible. Finally, for all the good times in the study room, thanks to the students at ODD at GFI, and to Sara, Lotta and Anna in room 305 at UNIS.

Frank Gaardsted

Contents

Chapter 1

Introduction

There is a growing amount of observational evidence of change in the Arctic Ocean and the Nordic Seas region (Dickson 1999). Reported changes in the Arctic include for instance a warming of the Atlantic layer (Grotefendt et al. 1998; Carmack et al. 1995), reduced ice thickness (Rothrock et al. 1999), reduction of multiyear ice area (Johannessen et al. 1999) and a retreat of the cold halocline layer in the Eurasian basin (Steele and Boyd 1998). In the Nordic Seas reduced formation of Greenland Sea Deep Water (Schlosser et al. 1991) and a possibly related warming of the deep waters (Østerhus and Gammelsrød 1999) are examples of reported change.

The Fram Strait is one of the main paths of exchange between the Arctic Ocean and the Nordic Seas, and thus a relevant area for monitoring and understanding the variability in the system (Schauer et al. 2004). Considerable progress has been made with respect to understanding ice transport through the Fram Strait (Vinje 2001), but the knowledge of long term variability of oceanic exchanges remains poor. Previous analyses of current measurements in the Fram Strait have mainly been limited to relatively short time scales, e.g. 1 to 3 years of transport estimates (Foldvik et al. 1988; Fahrbach et al. 2001; Schauer et al. 2004), or limited to studies of certain processes (Jonsson et al. 1992; Kasajima and Svendsen 2002). Here, based on the available current measurements from moored instruments, the possibilities of constructing longer time series of variability in the upper and intermediate layers of the East Greenland Current (EGC) in the period 1984-2000, are investigated.

Some of the main features of the Arctic Ocean / Nordic seas are briefly presented in chapter 2. An overview of the data sets are given in chapter 3. The best coverage was obtained in the period 1998-2000, and results from velocity measurements, hydrography measurements and transport estimates based on this data set are presented in chapter 4, chapter 5 and chapter 6 respectively. Chapter 7 deals with the possibilities for construction of transport estimates in periods with sparser data coverage. The two periods 97/98 and 84/85 are then discussed and compared to 98/00 in chapter 8 and

chapter 9 respectively. A few notes on mesoscale activity and large scale forcing are given in chapter 10. Finally, main conclusions are summarized in chapter 11.

Chapter 2

The Arctic Ocean / Nordic Seas

2.1 Bathymetry

Figure 2.1 shows a map highlighting the main bathymetric features of the Arctic Ocean and the Nordic seas. The Arctic Ocean is almost completely surrounded by continents. Two major deep basins, the Eurasian basin and the Canadian basin, make up the greater part of the central Arctic Ocean. These are separated by the Lomonosov Ridge which has a sill depth of about 1400 m. The deep basins are mainly surrounded by shallow continental shelves, relatively narrow from Alaska to Greenland and much broader eastwards from Spitsbergen (Barents, Kara, Laptev, East Siberian, Chuckhi seas). The surrounding land masses limit the exchanges with the rest of the world oceans to a few passages, the relatively shallow Bering Strait, Barents Sea and Canadian Archipelago, and to only one deep water connection, the Fram Strait (2600 m depth).

The Nordic Seas (the Iceland Sea, the Norwegian Sea and the Greenland Sea) also consists of several deep basins separated by various ridges. To the south the ridge between Greenland and Scotland, with a maximum depth of about 840 m (Hansen and Østerhus 2000), form a barrier that constrains free deep water exchanges between the Nordic Seas and the North Atlantic.

2.2 Exchanges through the Fram Strait

The arrows in figure 2.1 indicate some of the main features of the large scale circulation in the Arctic Ocean / Nordic Seas. The Fram Strait serves as an important pathway for waters both entering and exiting the Arctic Ocean. The eastern side, close to Spitsbergen, is dominated by the West Spitsbergen Current (WSC). This is the northernmost extension of the Norwegian Atlantic Current (NwAC) and represents a northward transport of sensible heat and salt from lower latitudes towards the Arctic (Aagaard et al. 1987). Before reaching the Fram Strait the Atlantic water enters

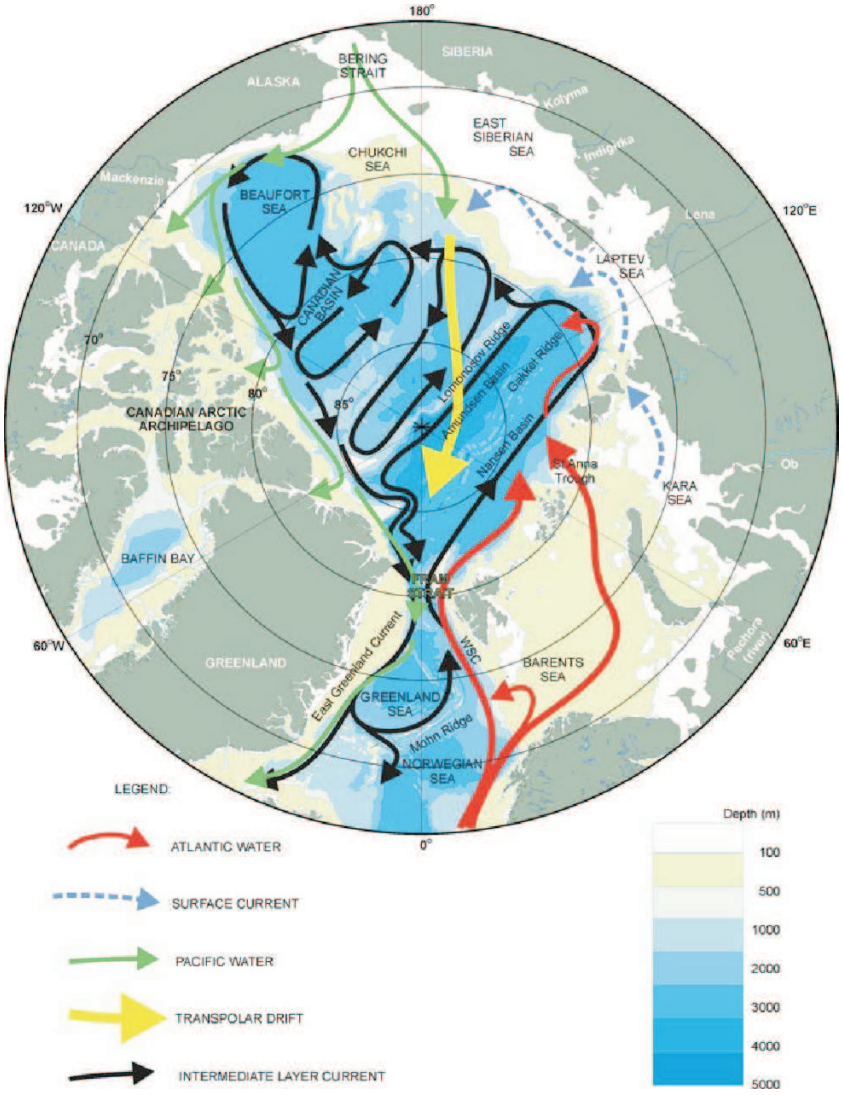

Figure 2.1: *Map of the Arctic Ocean and the Nordic Seas. The bathymetry is indicated by colors. The arrows show the main large scale current systems.*

the Nordic Seas through the Faroe-Shetland Channel and over the Iceland-Faroe ridge (Hansen and Østerhus 2000). It then flows northward as a part of the two-branched NwAC (Orvik and Niiler 2002). A further splitting of the NwAC results in one branch flowing eastwards into the Barents Sea while one branch continues northwards toward the Fram Strait as the WSC.

The dominating feature in the western part of the Fram Strait is the southward flowing East Greenland Current (EGC). The EGC is however not necessarily completely decoupled from the WSC, as the latter is known to split and partly recirculate in the Fram Strait (Aagaard et al. 1987; Rudels et al. 2000). Apart from the directly recirculating Atlantic Water in the EGC, strongly modified remnants of Atlantic water that actually did enter the Arctic Ocean, either through the Fram Strait or through the

Barents sea, return southwards in the EGC after having completed the various loops of the Arctic circulation (Aagaard 1989; Meinche et al. 1997).

Colder and less saline water also exits the Arctic Ocean with the EGC. In addition to a small inflow of relatively cold and fresh water through the Bering Strait, the Arctic Ocean receives large amounts of freshwater through precipitation and river runoff (Carmack 2000). Modifications occur through e.g. melting and freezing of sea ice. This polar water ultimately leaves the Arctic through the either the Canadian Archipelago or with the EGC through the Fram Strait.

The dominant hydrographic feature of the EGC is the Polar Front, which separates this cold, low-salinity polar water west of the front from the warmer and more saline Atlantic influenced water on the eastern side (Foldvik et al. 1988).

2.3 Water mass classification

A common water mass classification based on potential temperature and salinity, for the Arctic/Nordic Seas region, is the one first used by Swift and Aagaard (1981). Here, the somewhat simplified version of this classification from Foldvik et al. (1988) will be used (Table 2.1).

Table 2.1: *Classification of water masses relevant to the upper layers of the EGC (Adopted from Foldvik et al. (1988)). Note that this primarily is a classification for surface and intermediate water. Water with temperatures below* $0°C$ *at greater depths would be classified as Deep Water, not Polar Water.*

Water mass	**Temperature range**
Atlantic Water (AW)	$T > 3°C$
Arctic Intermediate Water (AIW)	$0°C < T < 3°C$
Polar Water (PW)	$T < 0°C$

Much more extensive classifications of water masses in the Fram Strait do exist (Rudels et al. 2002; Friedrich et al. 1995), but for easy comparison to Foldvik et al. (1988), and because temperature will be our main tracer, the simpler version (table 2.1) is sufficient.

Chapter 3

Current measurements

3.1 Main data set: 1998-2000

The most extensive data set of current measurements in the Fram Strait comes from 1997-2000 and was collected as a part of the European union funded project, Variability of Exchanges in Northern Seas (VEINS).

Figure 3.1 shows the positions of the moorings in the EGC in the Fram strait, from the two years 98/99 and 99/00. The exact positions of the moorings and their deployment and recovery times are listed in table 3.1. In 98/99, 6 moorings, sites A-F, were deployed. The following year moorings were redeployed at sites A-E. All the moorings were approximately aligned along 79 °N. The bottom profile is shown in figure 3.2. Mooring A was located on the Greenland continental shelf, close to the shelf break at about 280 m bottom depth. Moorings B,C and D were located over the slope at about 1000 m, 1800 m and 2360 m bottom depth respectively. The two easternmost moorings, E and F, were located at about 2480 m and 2580 m bottom depth respectively. The distance between the moorings varied from 20 km to 40 km.

The distribution of current meters on the moorings is shown in figure 3.2. The depth of each instrument is given in table 3.1. The vertical position and number of instruments on each mooring were approximately the same in the two deployment periods, forming 16 more or less continuous 2 year time series. The exceptions to this are the already mentioned mooring F, that was only deployed in 98/99, and due to instrument failure, the uppermost current meter at mooring D in 98/99 and the deepest current meter at mooring A in 99/00. The latter two are marked with crosses in figure 3.2. At these locations only 1 year long time series are available. The continuity is also slightly broken due to the time between recovery and redeployment of the moorings. This occurred in the latter half of September.

The current meters used were from Aanderaa Instruments (RCM7, RCM8 and DCM11) and Falmouth Scientific Inc. (3D-ACM). Inaccuracies in single measurements were between 0.5 cm/s to 1.0 cm/s. All instruments had a sampling interval of 1 hour.

More details about the mooring configurations are available in the reports by Fahrbach (1999) and Schauer (2000). Prior to the analysis all time series were low pass filtered to remove tides.

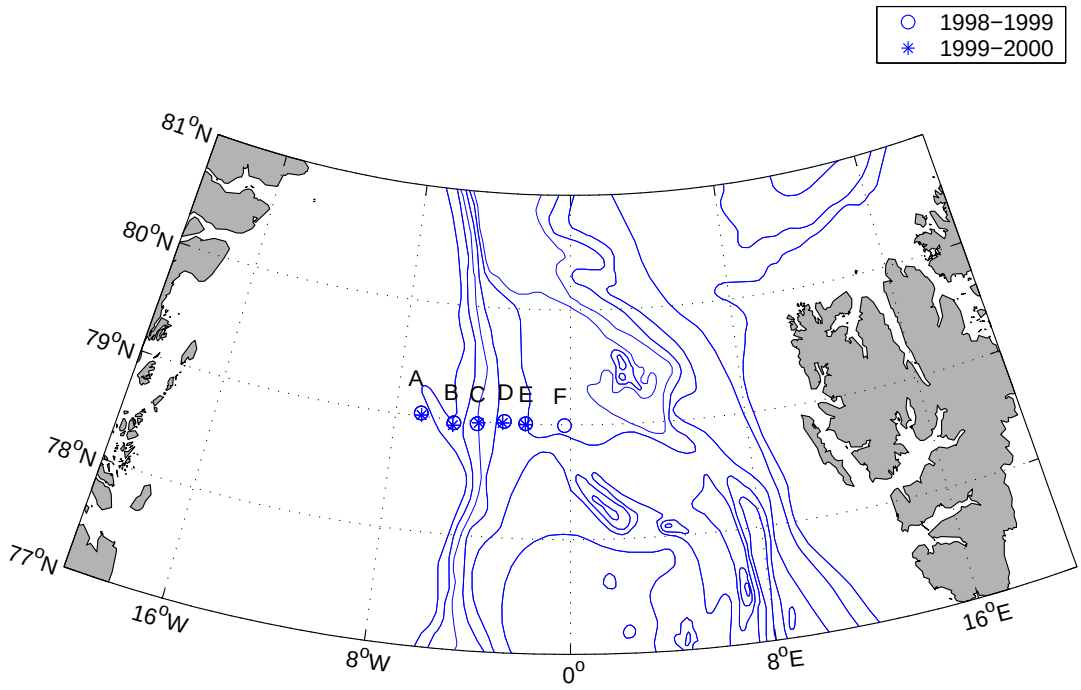

Figure 3.1: *Map showing the positions of the moorings. Moorings from 1998/1999 are marked ' ∘' and moorings from 1999/2000 are marked ' ⋆'. The letters A-F above each mooring will be used for reference to the moorings.*

3.2 Filling of gaps in the main data set

The result of a volume transport estimate through a section depends on the number of current meters used in the calculation, and how they are distributed in the section. Rather than using the largest common set of current meters from the two measuring periods, information from one period was used to construct the missing time series (crosses in figure 3.2) in the other period.

Table 3.1: Mooring details 1998-2000

Mooring	Time	Position		Instrument name	Instrument depth (m)	Bottom depth (m)
		Latitude	Longitude			
A	15.09.1998-16.09.1999	79°01.7‘N	06°50.8‘W	A1-98/99	64	280
				A2-98/99	270	
	27.09.1999-04.08.2000	79°00.6‘N	06°49.2‘W	A1-99/00	60	286
				-	-	
B	17.09.1998-16.09.1999	78°58.3‘N	05°18.7‘W	B1-98/99	50	1030
				B2-98/99	263	
				B3-98/99	1020	
	27.09.1999-04.08.2000	78°57.0‘N	05°21.1‘W	B1-99/00	45	967
				B2-99/00	221	
				B3-99/00	957	
C	17.09.1998-14.09.1999	78°58.8‘N	04°15.3‘W	C1-98/99	66	1795
				C2-98/99	271	
				C3-98/99	1475	
				C4-98/99	1785	
	25.09.1999-03.08.2000	78°59.4‘N	04°11.0‘W	C1-99/00	55	1828
				C2-99/00	301	
				C3-99/00	1507	
				C4-99/00	1818	
D	17.09.1998-14.09.1999	79°00.9‘N	03°01.1‘W	-	-	2365
				D2-98/99	246	
				D3-98/99	1450	
				D4-98/99	2355	
	26.09.1999-02.08.2000	79°00.1‘N	03°05.5‘W	D1-99/00	47	2365
				D2-99/00	243	
				D3-99/00	1449	
				D4-99/00	2355	
E	14.09.1998-14.09.1999	79°00.2‘N	02°02.6‘W	E1-98/99	76	2580
				E2-98/99	257	
				E3-98/99	1513	
				E4-98/99	2569	
	26.09.1999-02.08.2000	78°59.7‘N	02°03.3‘W	E1-99/00	68	2578
				E2-99/00	249	
				E3-99/00	1512	
				E4-99/00	2568	
F	13.09.1998-10.09.1999	78°59.6‘N	00°16.3‘W	-	-	2480
				F2-98/99	267	
				F3-98/99	1523	
				F4-98/99	2469	

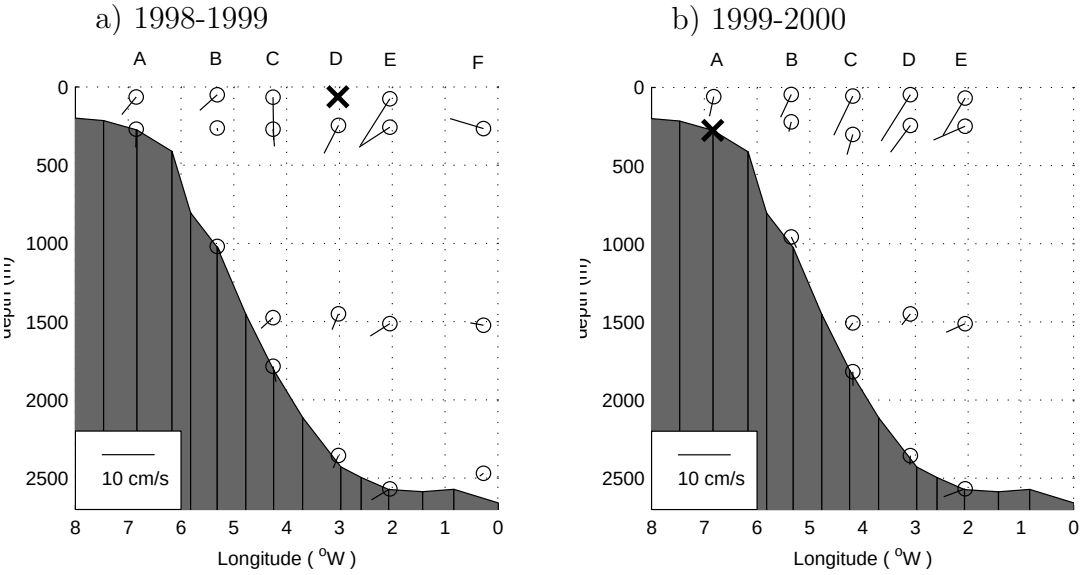

Figure 3.2: *Distribution of the current meters in the section. Left: 1998-1999, right: 1999-2000. The mean horizontal current speed and direction from each instrument are shown as vectors. Crosses mark positions where instruments failed, partly or completely.*

In 98/99 the uppermost instrument on mooring D failed. Figure 3.3 a) shows the time series of monthly mean northward velocity from the two uppermost instruments at mooring D (D1-99/00 and D2-99/00) for the 99/00 period. The magnitude was different, but the variability similar. This is confirmed in figure 3.3 b), which shows the regression of monthly mean cross section velocity from D1-99/00, on the monthly mean cross section velocity from D2-99/00. The correlation coefficient r is 0.92 and suggests linear estimation of the velocity in the upper layer based on the velocity below. The results from the 99/00 period are transferred to 98/99 and gives an estimated monthly mean velocity at the upper instrument

$$\hat{v}_{D1-98/99} = 1.2 \cdot v_{D2-98/99} - 3.1, \tag{3.1}$$

where $v_{D2-98/99}$ is the measured northward velocity in the second level from the surface for the 98/99 period. When the much noisier 6 hour mean values of velocities are used the correlation coefficient is of course lower (0.68).

The other spatial data gap is the deepest position on mooring A in 99/00, which due to a compass failure, only recorded the speed of the current and not its direction. Figure 3.4 a) shows a progressive vector diagram of measured current at 270 m at mooring A from 98/99 (instrument A2-98/99). Since the east-west component of the current was relatively small, possibly due to strong topographic control close to the bottom, the speed itself may perhaps be used to directly estimate the north-south component. Figure 3.4 b) shows the regression of monthly mean cross section velocity from A2-98/99, on the monthly mean speed from A2-98/99. The correlation coefficient

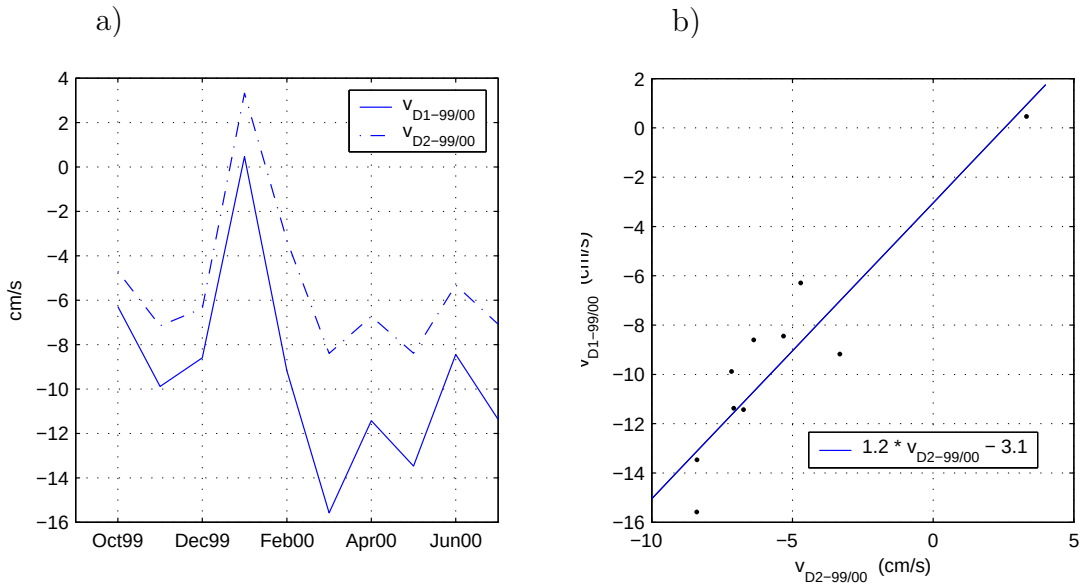

Figure 3.3: *a): time series of monthly mean southward velocity at the two uppermost current meters at mooring D for the 99/00 period. b): Regression of monthly mean cross section velocity from D1-99/00, on the monthly mean cross section velocity from D2-99/00.*

r using all points is 0.87. Excluding the one point (5.6,-2.2) that deviates considerably from a straight line fit gives $r = 0.99$. Assuming this last relation holds for the 99/00 period gives an estimated monthly mean northward velocity

$$\hat{v}_{A2-99/00} = -1.1 \cdot sp_{A2-99/00} + 0.9, \tag{3.2}$$

where $sp_{A2-99/00}$ is the monthly mean speed.

The gaps in the time series due to the recovery and redeployment of moorings were filled with the mean values at each location.

In the following we will focus on the upper 1500 m of the water column. If we include the two constructed time series in the data set, we have 14 time series, of 22 months length, of monthly mean cross section velocities at the positions marked by circles in figure 3.5. This constitutes the main data set and will be used for volume transport estimates. Although the depths of the upper and intermediate instruments were slightly different from one mooring to the next, upper instruments will be referred to as the 60 m level and the intermediate instruments as the 270 m level.

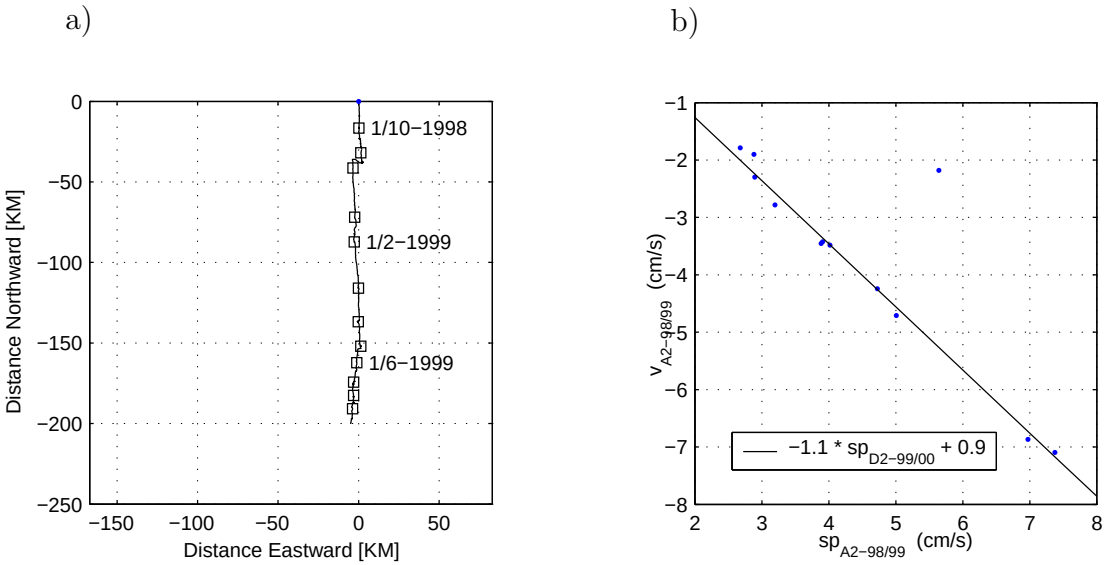

Figure 3.4: *a): Progressive vector diagram of velocity from the instrument A2-98/99. b) Regression of monthly mean cross section velocity from A2-98/99, on the monthly mean speed from A2-98/99.*

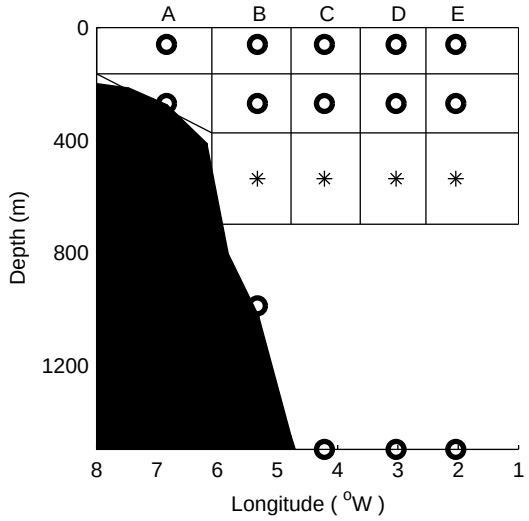

Figure 3.5: *The section through which volume transport is calculated. The circles show the positions of the actual current meters. The stars show the records constructed by interpolation (chapter 6).*

3.3 1997-1998

Figure 3.6 shows the positions of available current meters in the section from 1984 until 1998. For comparison, the main data set from 1998-2000 is included in the background.

The positions of the current meters from 1997-1998 are shown in Figure 3.6 a). This data set also comes from the VEINS measuring program and the number and positions of moorings and instruments deployed in our main area was the same as in 1998-2000. This makes it convenient to use the same notation when referring to moorings and instruments, e.g. the instrument at the westernmost mooring is referred to as A2-97/98. Still, since one entire mooring (D) was lost and three more instruments failed, the overall coverage was worse.

All 4 moorings were deployed on the 2'th and 3'rd of September 1997 and recorded continuously for about a year (between 360 and 365 days).

3.4 1990-1996

The Norwegian Polar Institute monitored ice thickness and velocity regularly in the Fram Strait since 1990 Vinje et al. (1998). Some of these moorings were also equipped with current meters. The positions of the instruments in the different periods are shown in figure 3.6 b).

3.5 1984-1986

Figure 3.6 d) shows the positions of the current meters in the section from summer 1984 until summer 1985 (Aagaard et al. 1985). We follow the notation of Foldvik et al. (1988), and refer to the westernmost mooring as FS1, the middle mooring as FS2 and the easternmost mooring as FS3. The positions of the moorings and the depth of the instruments are given in table 3.2. As a part of the same measuring program mooring FS1 were redeployed in 85/86 (Aagaard et al. 1988)(figure 3.6 c)). In addition one mooring, FS9b was deployed.

3.6 Supplementary hydrography data

Most of the moored instruments were also equipped with temperature sensors (Fahrbach 1999; Schauer 2000; Woodgate et al. 1998; Aagaard et al. 1985; Aagaard et al. 1988; Foldvik et al. 1988) that also sampled every hour.

In connection with the deployment and recovery of the moorings, CTD (Conductivity, Temperature, Depth) measurements along the section were carried out (Fahrbach 1999; Schauer 2000; Woodgate et al. 1998).

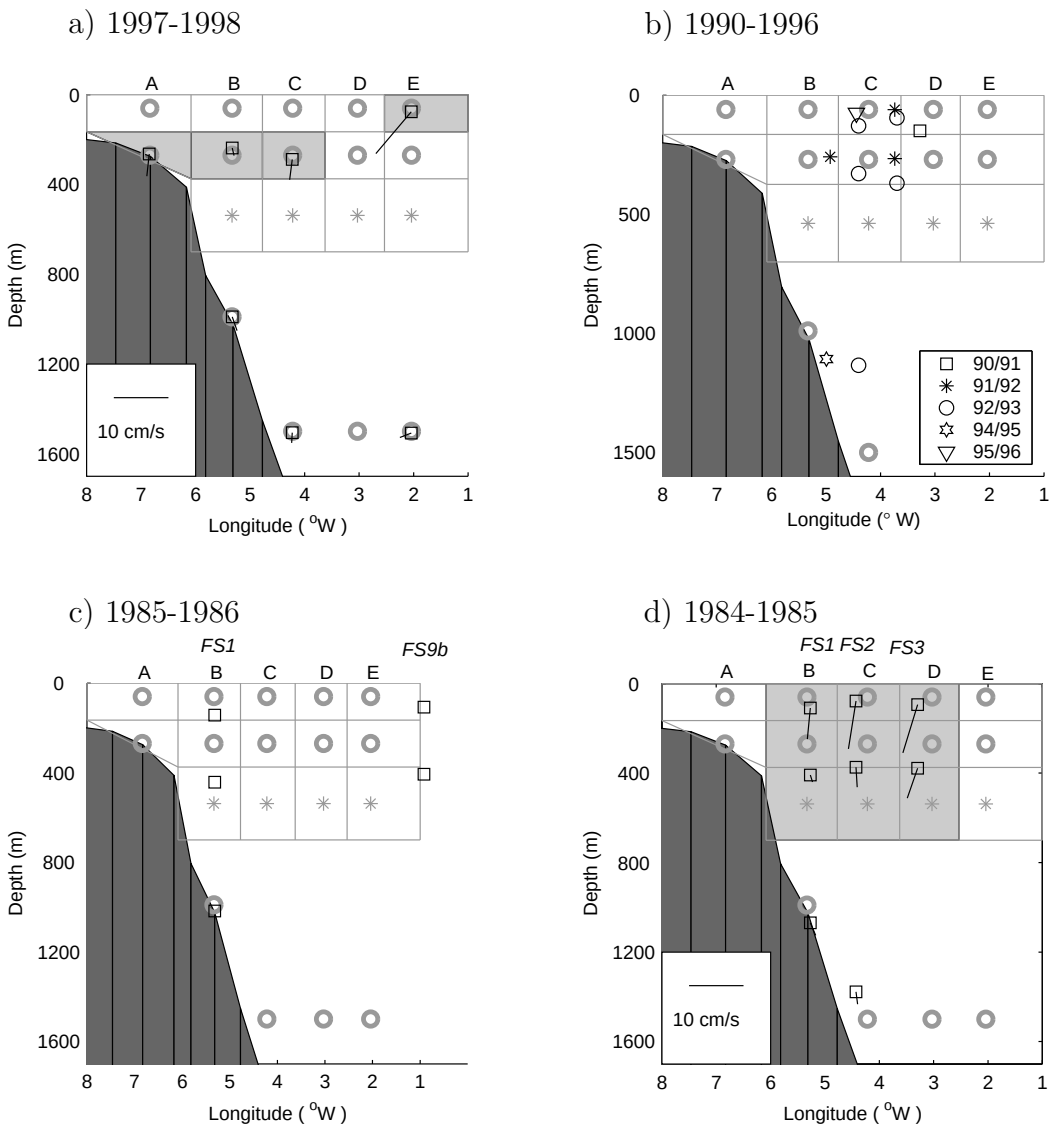

Figure 3.6: *Positions of current meters in the section in the periods a) 1997-1998, b) 1990-1996, c) 1985-1986 and d) 1984-1985. Squares mark the current meters in the different periods in a), c) and d). In b) various symbols are used for the different years (see box in the lower right corner). For comparison the 98/00 mooring array is also shown. The mean current at each instrument is shown as vectors in a) and d). Shaded areas in a) and d) mark the subsections used for volume transport estimates in chapter 8 and chapter 9.*

Table 3.2: Mooring details 1984-1985

Mooring	Time	Position		Instrument name	Instrument depth (m)	Bottom depth (m)
		Latitude	Longitude			
FS1	15.06.84-16.07.85	78°58.7‘N	05°16.1‘W	FS1-1	94	1094
				FS1-2	374	
				FS1-3	1069	
FS2	16.06.84-16.07.85	79°00.3‘N	04°25.7‘W	FS2-1	78	1678
				FS2-2	378	
				FS2-3	1378	
FS3	16.06.84-15.07.85	78°54,9‘N	03°17.7‘W	FS3-1	109	2359
				FS3-2	409	
				FS3-3	2334	

3.7 NCEP/NCAR reanalysis data

The atmospheric pressure data discussed in this thesis are from the NCEP/NCAR (National Centers for Environmental Prediction - National Center for Atmospheric Research) reanalysis. These are available electronically through the web site http://www.cdc.noaa.gov/.

Chapter 4

Results from current measurements 1998-2000

4.1 Annual means

The mean current speed and direction at each instrument, is shown as vectors in figure 3.2. The values are listed in table 4.1. For moorings A-D and the uppermost instruments at mooring E, the direction of the current was predominantly southwards. The rest of the current meters measured a stronger zonal current component than meridional. The two instruments F2-98/99 and F3-98/99 were the only ones with a mean northward component.

Figure 4.1 shows the mean v and u-components and their corresponding standard deviations calculated for the 98/00 period. The mean values were calculated from the main data set of monthly mean velocities (section 3.2), while standard deviations were based on 6 hour mean values of velocity. Shaded areas in in figure 4.1 a) correspond to southward velocities stronger than 5 cm/s. The core of the mean cross section current (v-component) seemed to be located in the upper 300 m, extending horizontally almost as far west as mooring B and at least as far east as mooring E (figure 4.1 a)). The overall maximum mean speed exceeded 9 cm/s and was recorded at the upper instrument at mooring D. Also the maximum mean southward speeds in the 270 m and 1500 m levels were found at mooring D, with magnitudes of about 5 cm/s and 2.5 cm/s, respectively.

In most of the section the mean u-component was negative, thus the zonal component of the current was mainly westwards (figure 4.1 c)). The westward velocity was strongest at mooring E and then gradually decreased westwards. Unlike the v-component, the u-component in the eastern part of the section varied little with depth. Farther towards the shelf the current was stronger in the surface layer than deeper down.

Figure 4.1 b) and d) show the standard deviations of the velocity components plotted as contours. For both components the variability was largest in the surface

Table 4.1: Mean temperature and velocities, together with their standard deviations (std), for the main data set.

Instrument	**Depth**	**u-component**		**v-component**		**Temperature**	
		mean (cm/s)	std	mean (cm/s)	std	mean (° C)	std
A1-98/99	64	-2.7	5.2	-3.6	7.4	-1.6	0.1
A2-98/99	270	-0.1	1.7	-3.8	3.9	0.7	0.3
A1-99/00	60	-0.8	0.4	-4.0	7.3	-1.7	0.1
A2-99/00	-	-	-	-	-	0.5	0.3
B1-98/99	50	-3.3	5.1	-3.2	7.6	-	-
B2-98/99	263	0.1	2.5	-0.6	3.3	1.3	0.5
B3-98/99	1020	0.7	1.4	-1.5	1.8	-0.1	0.1
B1-99/00	45	-2.0	5.4	-4.7	6.3	-1.8	0.1
B2-99/00	221	-0.5	4.7	-2.0	5.7	0.2	1.0
B3-99/00	957	1.0	1.6	-2.2	3.2	-0.1	0.1
C1-98/99	66	0,1	8.2	-8.8	8.5	-1.6	0.2
C2-98/99	271	0.3	4.2	-3.5	5.1	1.4	0.5
C3-98/99	1475	-0.2	1.4	-2.3	3.5	0.4	0.0
C4-98/99	1785	0.5	1.9	-3.2	4.9	-0.5	0.1
C1-99/00	55	-3.6	8.5	-8.1	8.3	-1.8	0.2
C2-99/00	301	-1.1	6.0	-4.1	6.4	1.5	0.6
C3-99/00	1507	-0.8	2.1	-1.3	3.4	-0,5	0.0
C4-99/00	1818	0.0	2.6	-2.9	5.9	-0.6	0.1
D2-98/99	246	-2.7	6.9	-5.8	7,3	1.7	0.5
D3-98/99	1450	-1.2	2.9	-3.3	3.8	-0.6	0.1
D4-98/99	2355	-1.0	5.0	-2.6	6.3	-0.8	0.0
D1-99/00	47	-5.5	8.8	-9.5	9.7	-1.5	0.7
D2-99/00	243	-3.8	5.8	-5.5	7.8	2.8	0.6
D3-99/00	1449	-1.7	4.8	-2,3	5.3	-0,5	0.1
D4-99/00	2355	-0.1	6.5	-1.9	8.4	-0.8	0.0
E1-98/99	76	-5.6	7.8	-9.6	9.1	0.4	1.5
E2-98/99	257	-5.8	7.8	-4.1	6.4	1.8	0.4
E3-98/99	1513	-3.7	4.1	-2.6	3.4	-0.7	0.1
E4-98/99	2569	-3.5	6.0	-2.3	5.0	-0.8	0.0
E1-99/00	68	-4.2	7.4	-7.7	9.3	-0.0	1.4
E2-99/00	249	-6.0	8.2	-2.8	7.4	2.2	0.6
E3-99/00	1512	-3.6	4.5	-1.7	4.0	-0.6	0.1
E4-99/00	2568	-4.1	5.5	-1.6	5.3	-0.8	0.0
F2-98/99	267	-6.3	7.6	2.1	7.0	1.9	0.4
F3-98/99	1523	-2.5	3.7	0.5	3.5	-0.7	0.1
F4-98/99	2469	-0.7	4.7	-0.6	4.0	-0.9	0.0

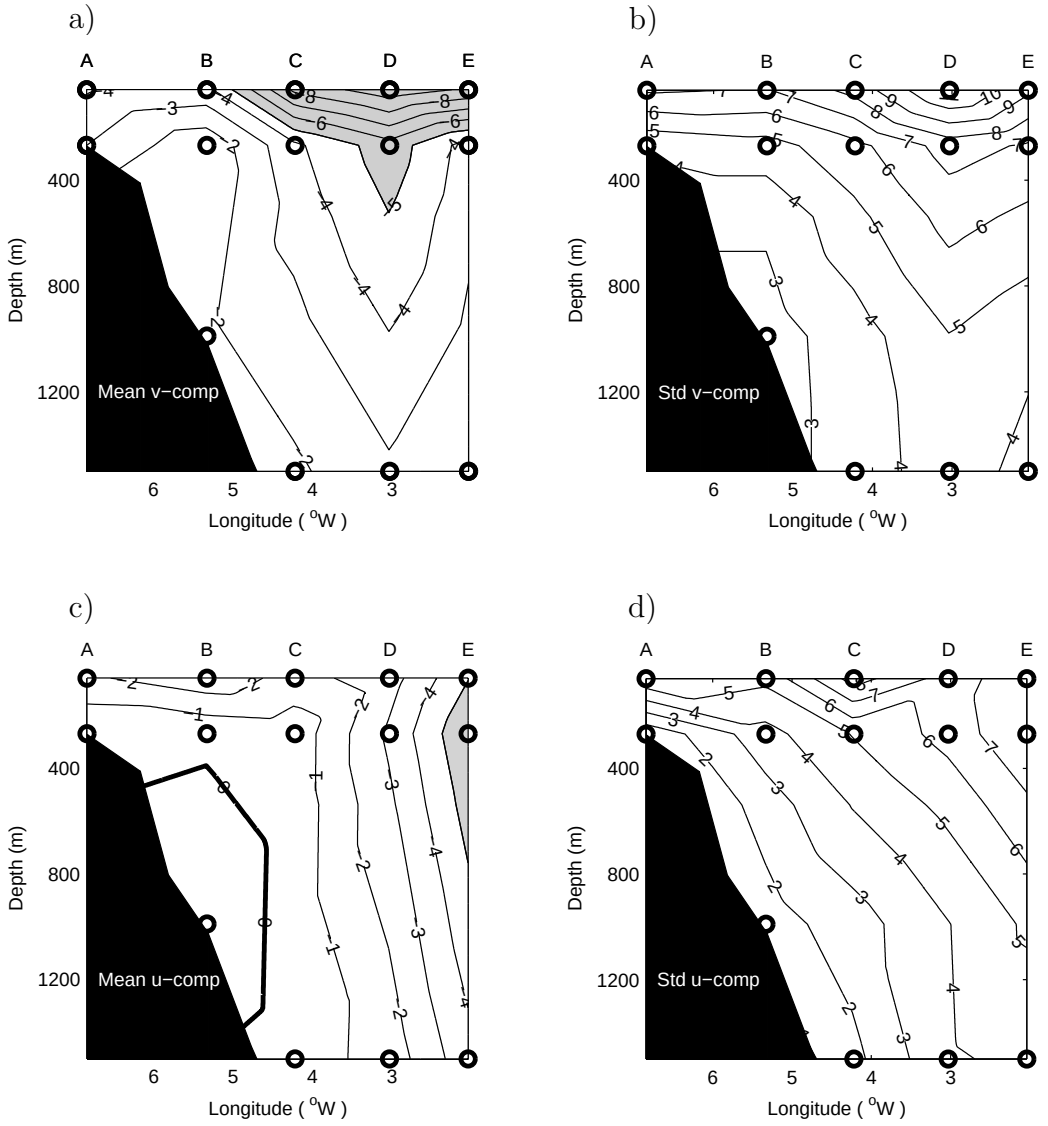

Figure 4.1: *Contour plots for the period 1998-2000. (a): Mean northward velocity (v-component). b): Standard deviations v-comp. c): Mean eastward velocity (u-component). d): Standard deviations u-comp. All numbers are are given in cm/s. The shaded areas in a) and c) mark velocities below -5 cm/s, i.e the strongest southward and westward currents. The circles show the positions of the current meters.*

layer. Generally, high absolute values of mean velocities are associated with high values of standard deviations, thus the positions with the strongest annual mean currents were also the positions with the strongest variability. Standard deviations based on monthly mean values of velocity give the same structure, but lower magnitudes.

4.2 Monthly means

To give an overview of the temporal variability, all the monthly mean cross section velocity fields from October 1998 until July 2000 are shown in figure 4.2. Although several months had a structure similar to the annual mean, the overall impression is that of a very variable current. The range of velocities was naturally larger than on annual timescales, even monthly mean northward current occurred.

Apart from months similar to the mean structure there were also months with a more bimodal structure. This is most clearly seen in the section from July 2000. The current was southward everywhere, but there were two stronger cores centered in the upper layers at mooring B and D. The same feature, although less pronounced can also be seen in the sections from March 1999 and October 1999. In March the easternmost core was much stronger than the western core. In October it was the other way around, with the western core slightly stronger than the eastern core. Tendencies of a similar bimodality is also found in July 1999, September 1999 and February 2000. These months the pattern was farther east with cores close to mooring C and E, again with variable strength of the cores.

Most of the northward part of the flow through the section occurred at mooring B. Six months gave a northward component on one or more of its three current meters. The vertical extent of this core varied, from including only one current meter in January and May 2000 to extending over the whole depth in August 1999. The strongest deviation from the annual mean field was found in January 2000. In addition to the relatively limited northward flowing core at about 270 m at mooring B, all the current meters at mooring D recorded a monthly mean northward current. Between these two there was a strong southward flowing core. Eastwards and westwards of mooring D and B respectively, the southward velocity again increased, making January 2000 the month with the largest cross sectional velocity gradients.

Several months the southward velocity increased from mooring D to mooring E (e.g. January 1999), indicating that the current was stronger farther east and that this mooring configuration might not be sufficient for monitoring the EGC. Still monthly mean values at mooring F (not shown) disprove the possibility of the core extending that far in 1998/99. On the western side of the section, several months show relatively high velocities at mooring A, indicating the possibility for some southward flow on the shelf

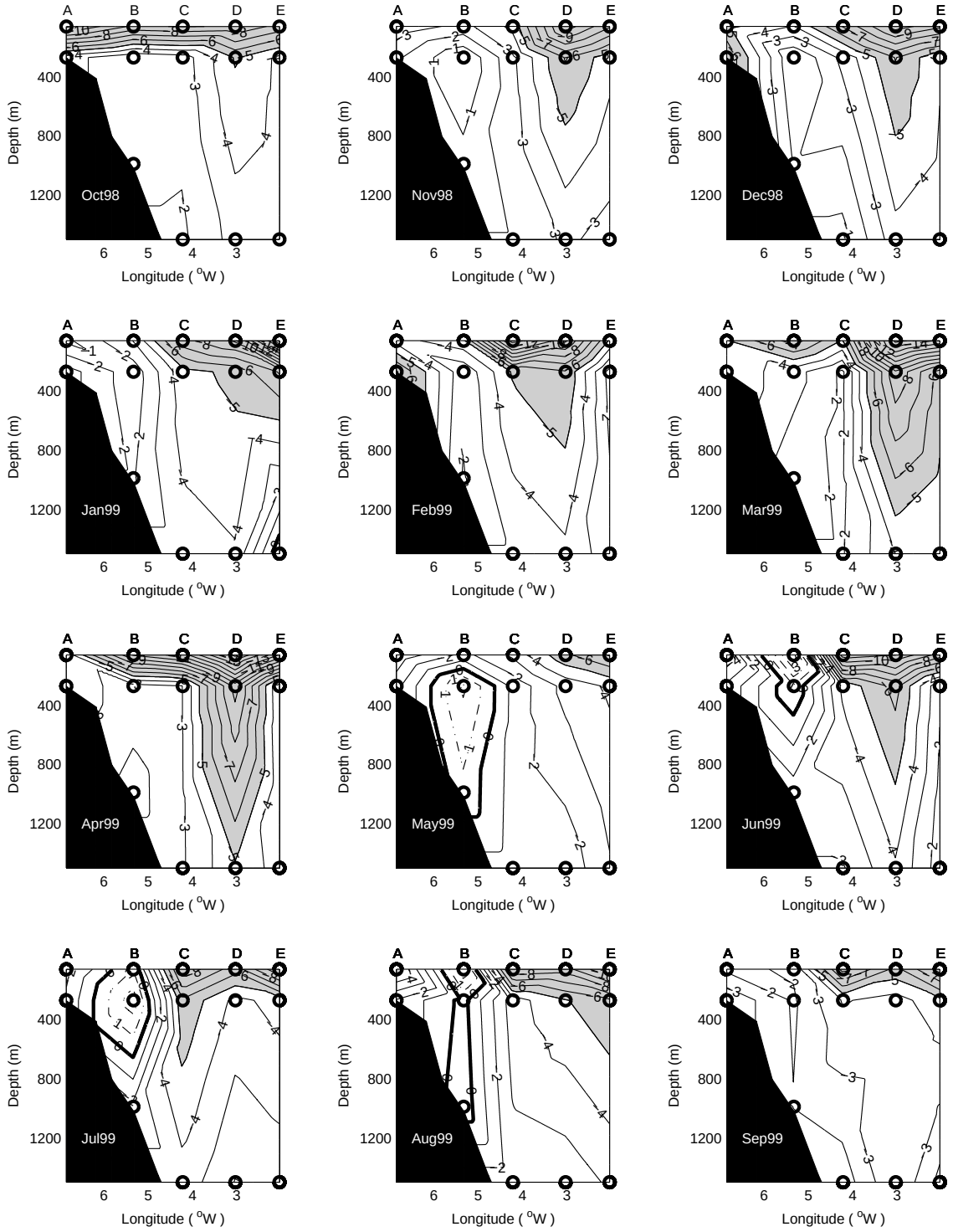

Figure 4.2: *Contour plots of monthly mean cross section velocity from October 1998 until September 1999. Shaded areas mark southward velocities stronger or equal to 5 cm/s. Solid lines mark negative contours and dashed lines mark positive contours. Thicker lines mark the zero contour.*

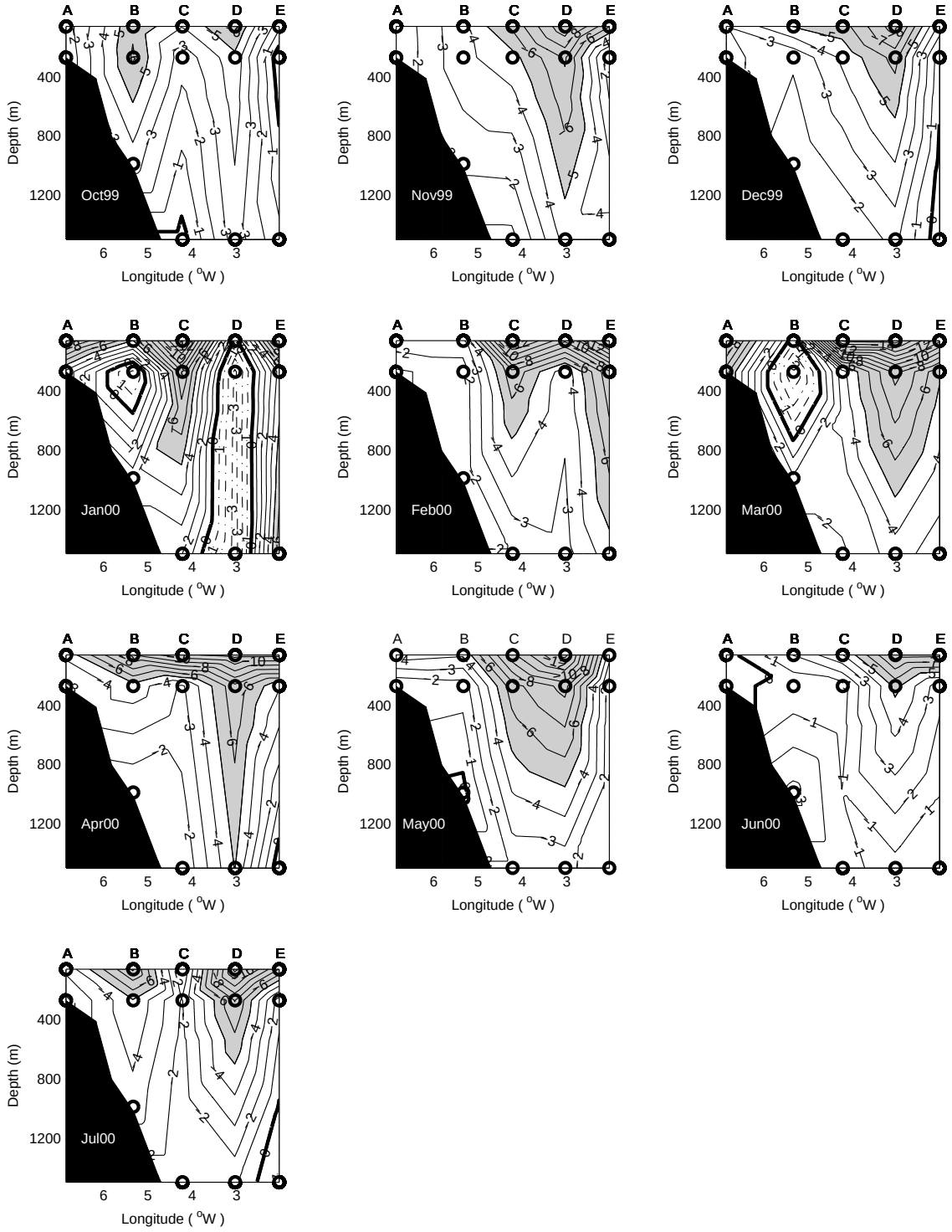

Figure 4.2: *continued. Contour plots of monthly mean cross section velocity from October 1999 until July 2000.*

Chapter 5

Hydrography 1998-2000

5.1 Time series of temperature

As a supplement to current measurements it can be useful to look at temperature and salinity measurements. In addition to being dynamically important because of their effect on density, they may also act as tracers and provide information about the origin of water masses. Most of the moored instruments were equipped with temperature sensors and provide time series of this at the positions of the instruments. The mean values of temperature together with the corresponding standard deviations from each instrument are listed in table 4.1.

The temperature at about 60 m depth is shown in figure 5.1 a). Due to instrument failures at the upper instruments at mooring B and D in the 98/99 period, only data from 99/00 are shown at this level. West of mooring D, monthly mean temperatures were very low, close to freezing, and thus falls in the PW category according to the water mass definitions in section 2.3. The temperatures at mooring D were slightly higher, but also below zero. Mooring E was situated right in the frontal zone between PW and AIW. The mean position of the front was however not necessarily constant. It seems like the extent of PW at this level increased throughout the period October 1999 to July 2000, i.e. the front moved eastwards. Also, mean values of temperature at the upper instruments at mooring E from both 98/99 and 99/00 (table 4.1) indicate that the front may have been even farther west in 98/99. The values are $0.4°C$ and $0.0°C$, for 98/99 and 99/00 respectively. The polar influence seems to have increased.

All the intermediate instruments provided good data and the time series at this level span the whole 22 month period. Figure 5.1 b) shows the monthly mean temperatures at about 270 depth for the period October 1998 until July 2000. Clearly the overall temperature characteristics here are very different from the near surface layer. The dominating water mass was the AIW, i.e. water with temperatures between $0°C$ and

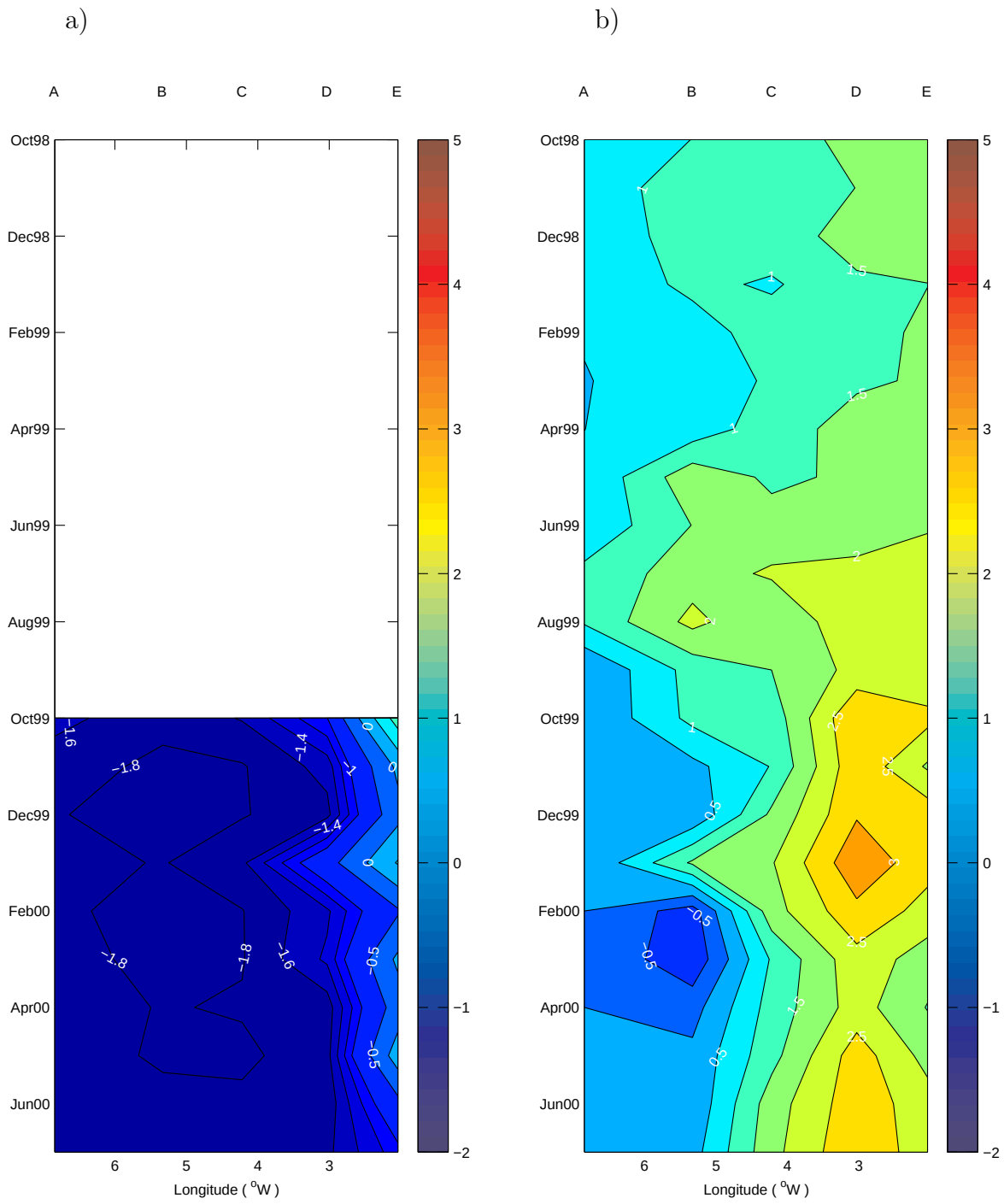

Figure 5.1: *Monthly mean values of temperature from moored instruments at the 60 m level a), and the 270 m level b), plotted as Hov-Möller diagrams. Due to instrument failures at the 60 m instruments at mooring B and D in the 98/99 period, only data from 99/00 are shown at this level.*

$3°C$ (section 2.3). As in the 60 m level the temperature increased eastwards. From October 1998 to about July 1999 the temperature difference between mooring A and mooring E was however relatively small, and a pronounced front did not exist. This situation changed in the latter half of the period, from August 1999 to July 2000. The temperature difference between the eastern and western part increased by at least $1°C$ and the transition was no longer smooth, but much more frontal like. This was due to both warmer water east of mooring C and colder water west of mooring C.

Water with monthly mean temperature characteristics outside the AIW range was only present in the period from January 2000 to April 2000. January was the only month in which one of the instruments recorded a monthly mean temperature above $3°C$, i.e. the characteristics of AW. This occurred at mooring D. Note that the time of this event coincided with the only time of monthly mean northward current at mooring D (figure 4.2). From February to April temperatures dropped below zero at mooring A and B, and these were the only months and positions with PW characteristics at 270 m depth. Still, the fact that the temperature in the western part in general was lower in the latter half of the measuring period may indicate that the PW extended deeper.

5.2 CTD-measurements

The temperature sensors mounted on the moorings provide important information about the temporal variability at individual positions, but not really enough about the spatial structure. CTD-measurements on the other hand, provide detailed snapshots of the spatial structure at a moment in time.

The figures 5.2 a), c) and e), show sections of potential temperature at $79°N$ between $8°W$ and $1°W$. The stations were occupied in August 1998, September 1999 and August 2000, i.e. just before, in the middle of, and immediately after the time series of temperature in figure 5.1. The positions of the current meters that constitute the main data set of current measurements are also shown. The thick white lines in the temperature sections mark the zero contour and thus, according to the water mass definitions in section 2.3, separate the PW from the AIW.

The upper instruments at the three westernmost moorings were in PW in all the sections, while as we also noted from the time series, the variability was much stronger in the eastern part. Consider for instance the upper instrument at mooring E. It was close to the front in 1998 and in 1999, but in both cases on the warmer side. In 2000 however, this position was completely dominated by PW. The vertical extent of PW also varied considerably from section to section. West of mooring D, the depth of the zero isotherm was between 100 m and 150 m in summer 1999, and between 200 m and 250 m in 2000. Although the latter is a snapshot, it does confirm the impression that the amount of PW in the section did increase during 99/00.

Figure 5.2 b), d) and f) show the corresponding sections of salinity. In general

low temperatures were associated with low salinities. There was also a pronounced salinity front between the PW and the AIW and the position of this front coincides roughly with the temperature front. The relatively fresh surface layer is probably due to seasonal melting. During the freezing season a homogeneous mixed layer is more likely.

Both the time series of temperature in figure 5.1 and the monthly mean values of velocity, show strong month to month variability at 270 m depth. This is also reflected in the CTD sections. In both 1998 and 1999 there were several cores of relatively warm and saline water surrounded by areas with colder and fresher water, while in 2000, there was a more continuous intrusion of warmer water. Again these may possibly not have been long term features, but rather related to the strongly varying velocity field.

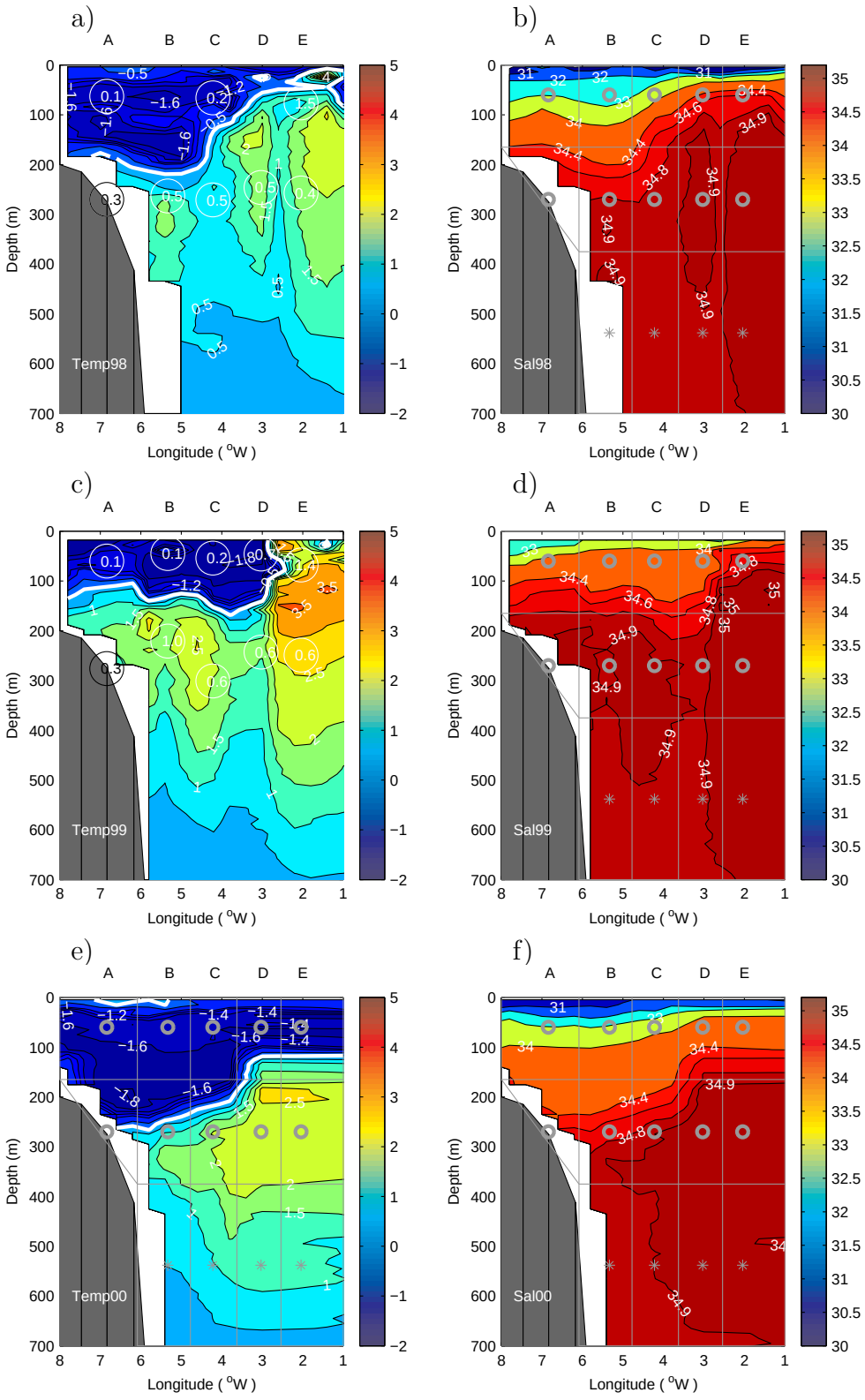

Figure 5.2: *Sections of potential temperature and salinity from summer 1998 (a) and b)), 1999 (b) and c)) and 2000 (e) and f)). Thick white lines mark the zero contour. The circles in a) and c) mark positions of moored instruments that provided temperature data. Instruments from 98/99 are shown in a) and instruments from 99/00 are shown in c). The numbers in the circles are the standard deviation of temperature at the corresponding instrument, based on 6 hour mean values.*

Chapter 6

Volume transport 1998-2000

6.1 Estimation of volume transport

A measure of the overall strength of the current is given by the volume transport, simply defined as the volume of water flowing through a section (an area) per unit time. For comparison to Foldvik et al. (1988), the volume transport was calculated through the section shown in figure 3.5, extending horizontally from 8 °W to 1 °W and vertically from the surface down to 700 m depth. The actual calculation was carried out by dividing the section into smaller sub sections, with one current record in each, letting this represent the velocity in the sub section. The transport in each section was then estimated as the product between the cross section velocity and the sub section area. In the two uppermost levels actual current measurements were available, but in the lowermost level interpolation was necessary. This was done using linear interpolation between the measured velocities directly above and below the level which was estimated. Where nothing else is stated numbers are given in Sverdrups (Sv), which corresponds to $10^6 \times m^3/s$.

6.2 Total transport

Figure 6.1 a) shows the time series of the estimated monthly mean southward volume transport. The mean transport for the whole period was 3.7 Sv. In t98/99 the transport was slightly higher (3.8 Sv) and in 99/00 slightly lower (3.5 Sv). The month to month variability was much larger and monthly mean transport values range from just above 2 Sv to above 5 Sv. It is difficult to draw any conclusions about seasonal variations from a 22 month time series. Still, there are some features that support the possibility of a seasonal signal in the EGC. Both years had maximum transport in late winter / early spring followed by transport minima shortly after, in late spring / early summer.

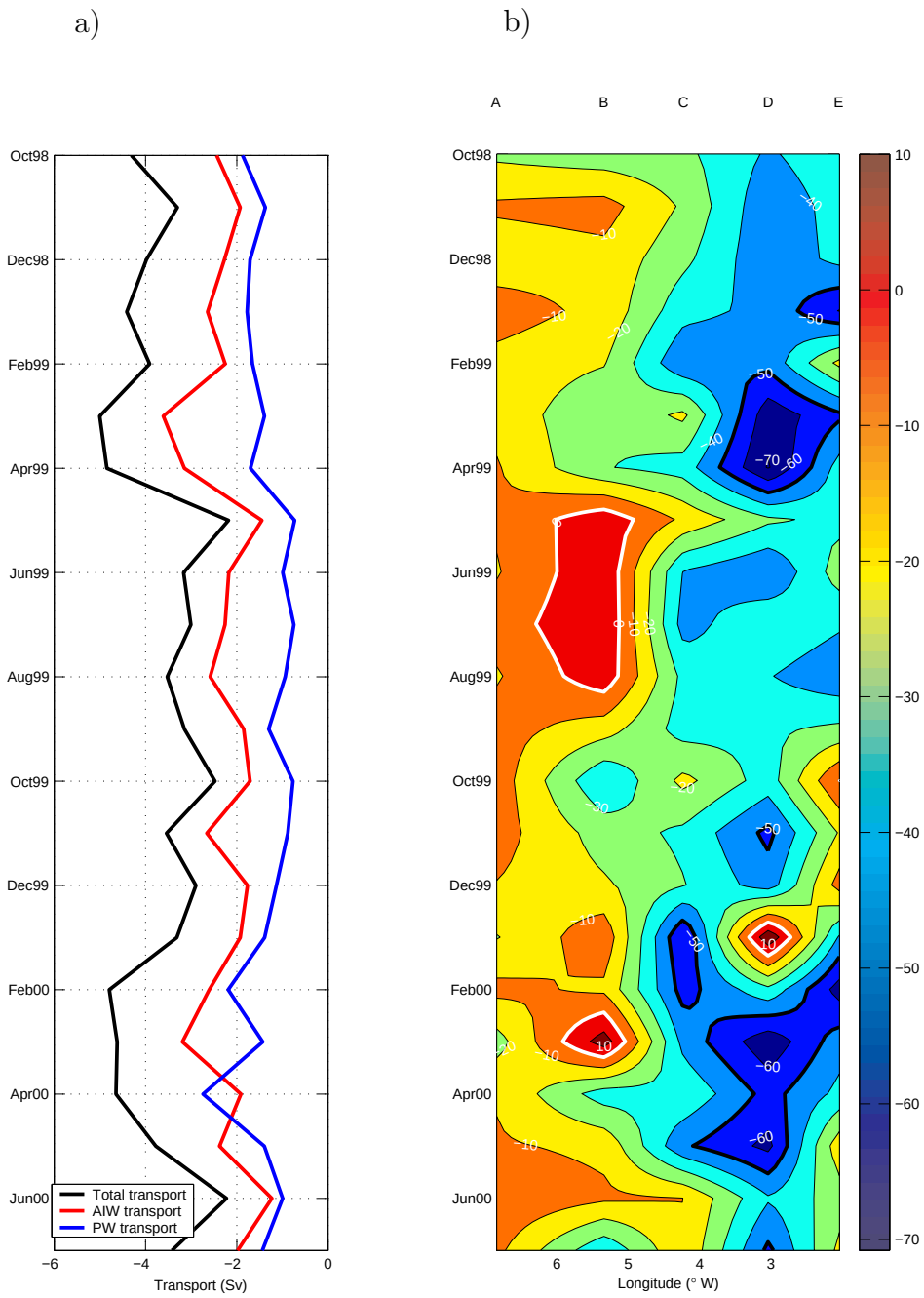

Figure 6.1: *a): Volume transport estimates in Sv for the main period. Negative values mean southward transport. The black curve shows the total transport, the red curve shows the AIW transport and the blue curve shows the PW transport. b): Hov-Möller diagram of vertically integrated transport. The numbers are given in m^3/sm. Thick black lines mark positions and periods with the strongest southward transport. Thick white lines mark positions and periods with net northward transport.*

Figure 6.1 b) shows a Hov-Möller diagram of vertically integrated transport, and gives an impression of how the transport was distributed in the section. Thick black lines mark positions and periods with the strongest southward transport. Thick white lines mark positions and periods with net northward transport.

The contribution to the net southward transport was in general largest in the eastern part of the section and also the increases in transport in late winter / early spring were due to increased velocities in this area, especially at mooring D. The duration of this increase was shorter, but the magnitude stronger in 1999 than in 2000. The reversal of the flow in January 2000 at mooring D did contribute to a relatively small net transport this month, but a simultaneous strengthening of the southward transport at mooring C, to an overall maximum, reduced the effect of the reversal. Apart from these extreme events the vertically integrated transport at the three easternmost moorings was fairly constant throughout the 22 month period. Farther west the relatively common occurrences of northward monthly mean velocities at mooring B gave several months with net northward transport in this region. This was for instance the case in summer 1999, contributing to making this a period of small total net transport through the section.

6.3 Transport of PW and AIW

It is also interesting to try to calculate the transport of the various water masses in the section. Again we followed Foldvik et al. (1988) and separated the water into only two classes, PW and AIW. We used the same division of the section as shown in figure 3.5. In subsections where the monthly mean temperature, according to the moored instrument, was below zero, the transport was added to the PW transport, where it was above zero the transport was added to the AIW transport. In the interpolated level where there were no instruments (stars in figure 3.5), we assumed AIW characteristics. This was at least the case in all the CTD transects in section 5. The temperatures at the upper instruments at mooring B and D in 98/99 are unknown due to instrument failures. We solved this by interpolating linearly between the moorings east and west of these positions.

The resulting estimated transports of PW and AIW are shown in figure 6.1. The red curve represents the AIW and the blue curve represents the PW. These two added together equal the total transport (black curve). The mean southward transport of PW was 1.4 Sv and the mean southward transport of AIW was 2.3 Sv. The only month with larger PW transport than AIW transport was April 2000. This is mainly due to the large vertical extent of PW in spring 2000 (figure 5.1 b)).

6.4 Heat transport

There is also major interest in the heat budgets of both the Arctic Ocean and the Nordic Seas (Simonsen and Haugan 1996). An important part of these budgets is the advection of heat with ocean currents. We followed Simonsen and Haugan (1996) and used a reference temperature T_{ref} of -0.1 ° C. The specific heat c_p of sea water is approximately 4000 $J/(degkg)$. The density ρ was taken to be 1028 kg/m^3. The heat transport H through a sub section is then given by

$$H = vAc_p\rho(T - T_{ref}),$$

where v is the monthly mean cross section velocity through the sub section, A is the subsection area and T is the monthly mean temperature in the section.

Figure 6.2 shows the estimated monthly mean northward heat transports through the section. The black curve shows the total heat transport. The mean value is -6.3 TW, i.e. relative to $-0.1°C$ the EGC transported heat southwards. If we look at the PW and the AIW separately, the transport of PW, due to temperatures lower than the reference temperature, represented a positive northward transport of heat, and the AIW ($T > -0.1°C$) represented a southward transport of heat. The mean values are -6.9 TW and 13.2 TW for PW and AIW respectively.

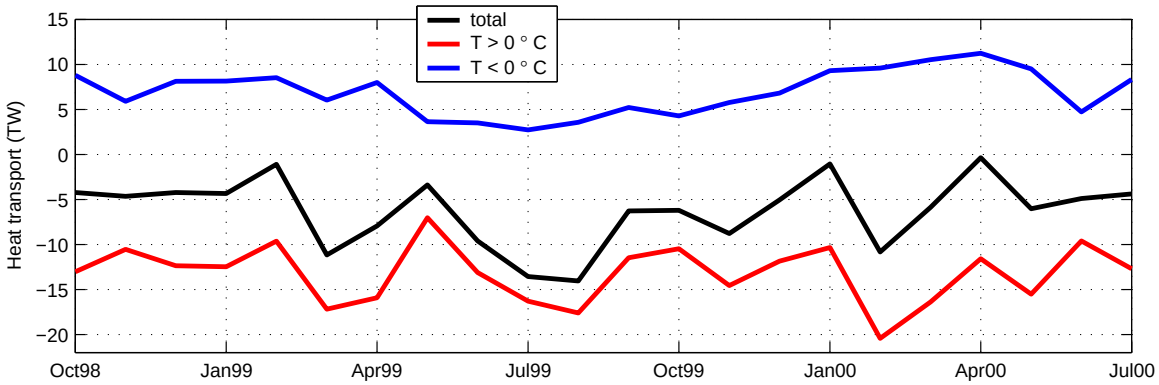

Figure 6.2: *Heat transport estimates relative to $-0.1°C$. The black curve is the total heat transport, the red and blue curves are the heat transports by AIW and PW respectively. Negative values indicate a southward transport of heat.*

The various transport estimates in this chapter are listed in table 6.1.

Table 6.1: *Summary of the various transport estimates.*

	Volume transport (Sv)			Heat transport (TW)		
Period	**Total**	**PW**	**AIW**	**Total**	**PW**	**AIW**
1998-2000	-3.7	-1.4	-2.3	-6.3	6.9	-13.2
1998-1999	-3.8	-1.4	-2.4	-7.1	6.1	-13.2
1999-2000	-3.5	-1.4	-2.1	-5.4	7.7	-13.2

6.5 Errors in the transport estimate

Random instrumental errors are believed to be small since monthly mean values are calculated from a large number of individual samples (Fahrbach et al. 2001; Ingvaldsen et al. 2004a). For this data set, systematic errors have been taken care of by the calibration (Fahrbach et al. 2001).

There are several other possible sources of errors in the transport estimates. Rather than to make one overall error estimate that is supposed to include all, it may be more enlightening to look at some of the main problems individually. The errors discussed below were calculated from the mean velocity field. They do not apply to monthly mean transport estimates.

Consider for instance the eastern and western boundaries of the section. In our estimate we assume that the velocity there is equal to the velocity at mooring E and mooring A respectively. If we instead e.g. assume that the true velocities between mooring A and the western boundary, and between mooring E and the eastern boundary, approach 0 cm/s linearly this reduces the mean southward transport by 0.5 Sv.

Another possible problem is the fact that we have no measurements between 270 m depth and 1500 m depth in the central and eastern part of the section. In the transport estimates, linear interpolation between these levels was used. A worst case error associated with this assumption can be obtained by replacing the interpolated values with the actual measured values in the levels below and above. This gives a maximum error of 0.4 Sv. Errors associated with the interpolation implied by the representation of the section as boxes with constant velocity, are of the same order of magnitude. In general the errors that arise due to interpolation will be largest when the velocity difference between the instruments are large.

Woodgate et al. (1999) found the baroclinic Rossby radius in the EGC at $75°N$ to be about 7 km, i.e. far less than the distance between the moorings. If this value is representative of the EGC in the Fram Strait as well, this may, especially in the

monthly mean transports enlarge the uncertainty.

For annual mean values of velocity the error in the estimated mean is small due to the large number of samples. On monthly mean values however, this error will be larger.

The errors related to calculation of the total volume transport also apply to the estimates of PW and AIW transports. Note however that additional uncertainty is introduced due to the poor resolution of the temperature field when this is based only on data from moored instruments. In terms of separating the PW from the AIW it is the position of the zero isotherm, the front, that is important. Of course this does not necessarily follow the artificial sub division of the section used above to estimate the transport. The position of the front may vary substantially without effecting our estimates of PW transport and AIW transport.

Chapter 7

Extending the time series of volume transport

7.1 Correlation analysis

Due to the sparser spatial coverage in the 1984-1998 period (figure 3.6), the method for estimating transports used above is not likely to produce good results for these years. Can reliable transport estimates be made using data from fewer instruments? Woodgate et al. (1999) and Orvik and Skagseth (2003a) successfully calculated transports in the EGC at 75° N and in the Norwegian Atlantic slope current (NwAsC) respectively, using only one current meter, while Ingvaldsen et al. (2002) needed data from two current meters to produce good transport estimates in the Barents Sea opening.

To see how variability in individual current records related to the variability in the total transport in the EGC in the Fram Strait, each record was correlated to the total transport for the 1998-2000 period. The results are shown in figure 7.1. Shaded areas mark correlations higher than 0.6. For the 98-99 period the correlation field shows two areas with correlation coefficients larger than 0.6 (figure 7.1 a)), at mooring B and mooring D, in both cases the vertical extent is from the surface all the way down to 700 m. The overall highest correlation is found at 270 m depth at mooring B with values exceeding 0.9. Intuitively this corresponds well to the results found in chapter 6, figure 6.1 b), where the southward transport increase in late winter / early spring in 1999 was due to an increase at mooring D, while the following decrease in late spring / early summer was due to a reversal at mooring B. The transport in this period could have been relatively well estimated using two intermediate from mooring B and mooring D.

The situation in 99/00 was completely different (figure 7.1 b)). The overall highest correlation between velocity at individual instruments and total transport in this period is just above 0.7 and occurs at the upper instrument at mooring C and at all instruments at mooring E. At both mooring B and D, which had relatively high correlations for

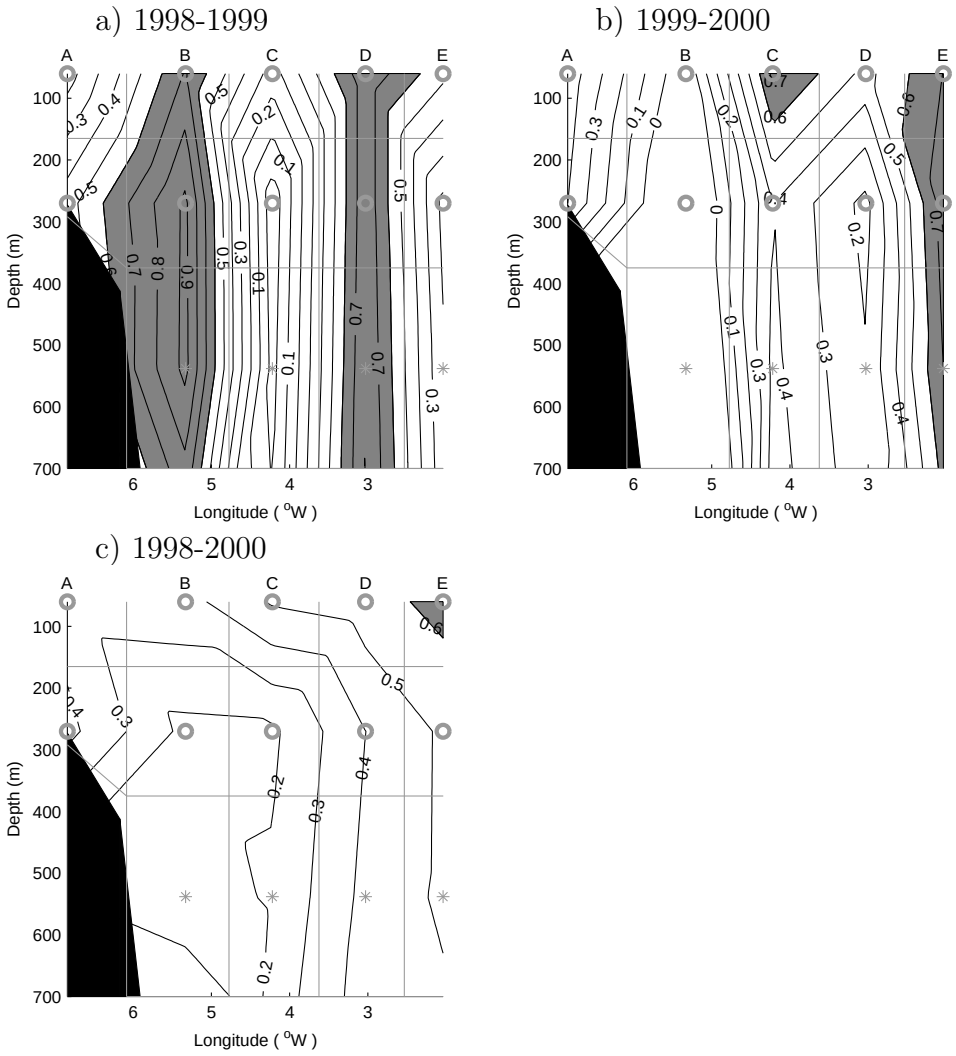

Figure 7.1: *Contour plots of correlation between monthly mean values of cross section velocity at individual instruments and monthly mean values of transport. a) for the period 1998-1999, b) for the period 1999-2000 and c) for the period 1998-2000. Shaded areas mark correlations higher than 0.6. The positions of the current meters are marked as circles.*

the 98/99 period, the correlations in 99/00 are not significantly different from zero. The pattern of relatively high correlations are shifted eastwards in 99/00 compared to 98/99. Figure 7.1 c) shows the correlations for the whole period. As expected, due to the differences outlined above, this does not produce any higher correlations.

7.2 EOF-analysis

The discussion in the previous section indicates that much of the monthly mean variability at individual instruments is not directly related to variability in the monthly mean transport. A simple Empirical Orthogonal Function (EOF) analysis may provide

a better understanding of what is going on. This is a method of separating the total variability in data sets into modes of uncorrelated (orthogonal) standing oscillations (appendix A). The results are a number of spatial structure fields (the EOF's) and a corresponding time evolution for each field (the principal components).

Figure 7.2 shows the first two EOF modes along with their principal components, based on monthly mean values of cross section velocity. Together they explain more than half (53 %) of the variance. These modes are mathematical constructions and not necessarily representative of any physical processes. In this case the second mode, shown in figure 7.2 b) most strongly resembles an actual observed feature. With maximum values at the uppermost instrument at mooring D, and decreasing values both downwards, eastwards and westwards of this, the structure of the second mode is very similar to the mean velocity field in figure 4.1. The principal component of this mode is shown in figure 7.2 d). It correlates by $r = 0.82$ to the total volume transport shown in figure 6.1. It seems like much of the variability in the monthly mean transport was associated with variability in the strength of a structure similar to the mean velocity field.

The first EOF, which accounts for 31 % of the variance, is shown in figure 7.2 a). The sign of the field shifts from positive at moorings A, C and E, to negative at moorings B and D, i.e. it does not seem to contribute very much to net transport variability. Still, since it explains such a large fraction of the total variability, it does certainly complicate estimation of the net transport by e.g. regression estimates based on single instruments.

The next three EOF's explain 15 %, 14 % and 7% of the variance. Although possibly significant they will not be discussed here.

Based on the above analysis and the data coverage from 1984 to 1998 (figure 3.6) it is evident that reliable transport estimates for large parts of this period is unrealistic. The structure of the current is too variable, and a much more extensive coverage seems necessary. Still, if one were to monitor the EGC using a reduced data set we may get a few ideas on how these instruments should be distributed in the section to obtain the best results. The relatively successful linear estimation of velocity at the upper instrument at mooring D in the 98/99 period, based on the velocity at the instrument below (section 3.2), is due to the fact that the correlation between monthly mean values of velocity between instruments at the same mooring is relatively high. This is also reflected in the correlation fields (figure 7.1) where lines of constant correlation are mainly vertical. Regarding volume transport estimates, it seems like a good horizontal resolution is more important than a good vertical resolution. E.g. four suitably placed moorings with one instrument each would provide more information, than one mooring with four instruments.

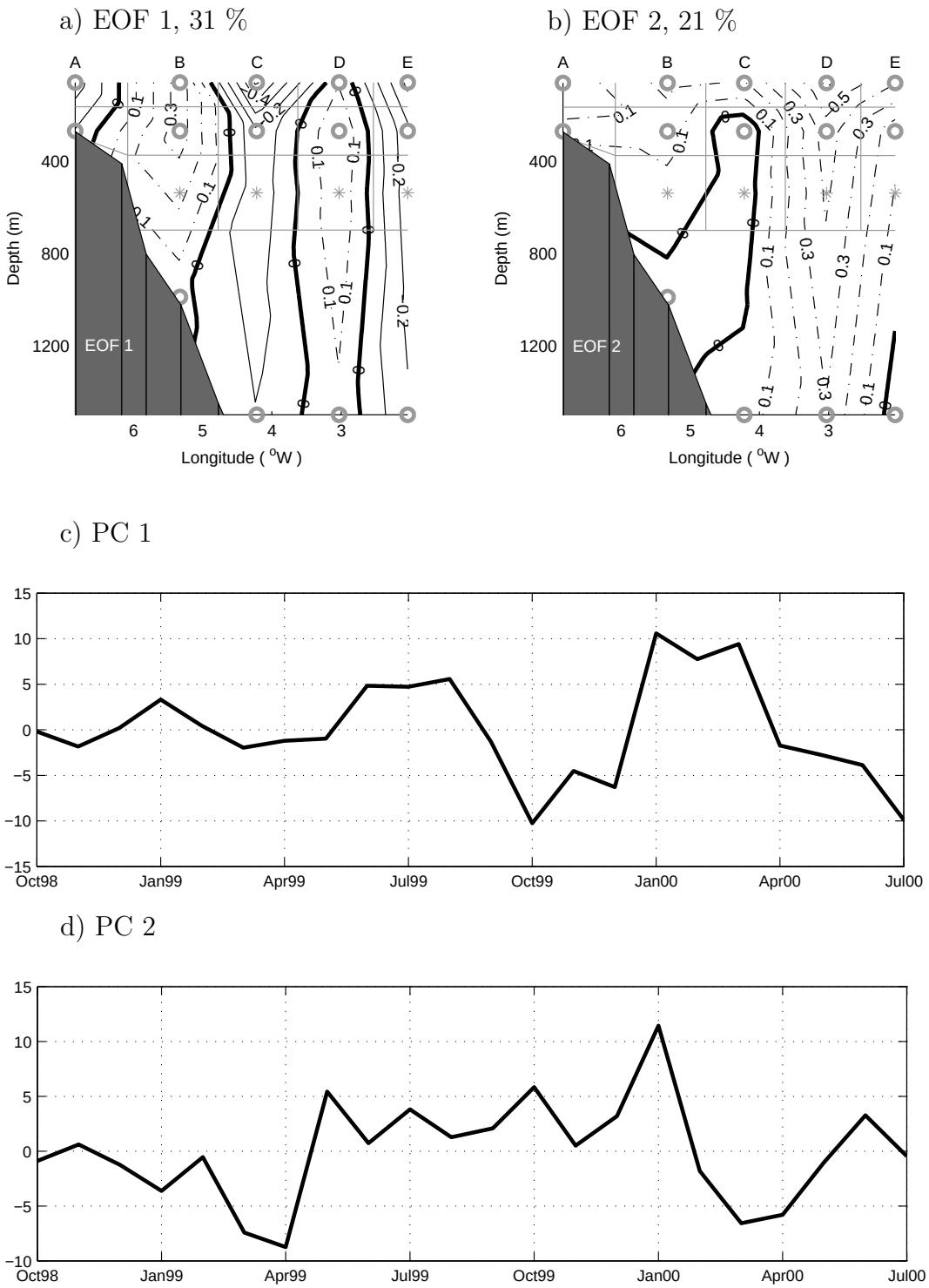

Figure 7.2: *Results from the EOF analysis based on monthly mean values of cross section velocity. a) the first EOF mode, explaining 31 % of the variance, b) the second mode, explaining 22 % 0f the variance. Full lines mark negative contours, stippled lines mark positive contours and thick lines mark the zero contour. The principal components for the first and second modes are shown in c) and d) respectively.*

Chapter 8

1997-1998

8.1 Volume transport

Based on the correlation analysis in the previous section (7.1) and the instrument coverage in 97/98 (figure 3.6 a)), we now try to estimate the transport in 97/98 by using one instrument from each mooring (A2-97/98, B2-97/98, C2-97/98 and E1-97/98). The relationship between the variability in the cross section velocity at these four locations and the total transport was found for the 98/00 period and then transferred to the 97/98 period. Figure 8.1 a) shows the regression of total monthly mean southward

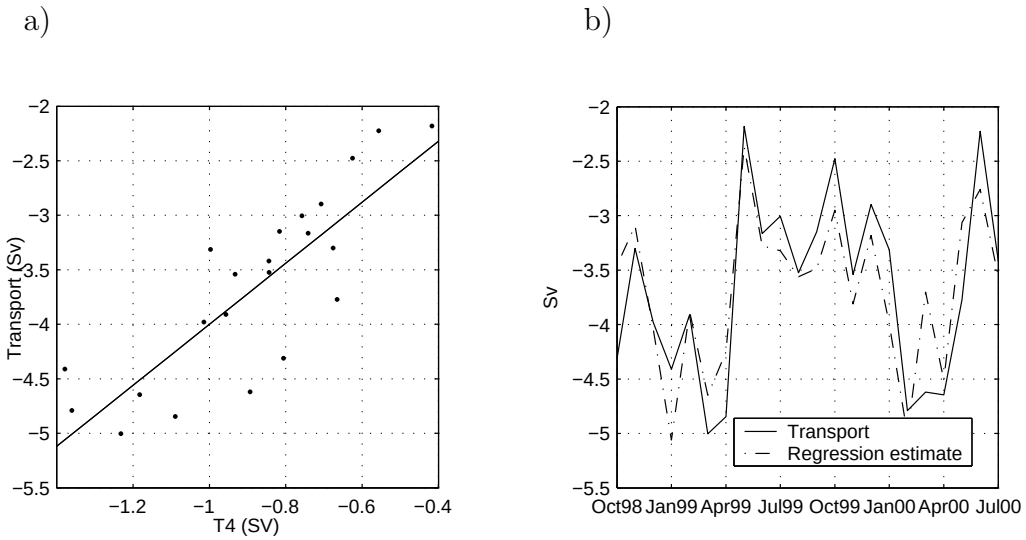

Figure 8.1: *a): Regression of total transport on the sum of the transport in the four shaded areas in figure 3.6 a). b): Transport based on all current records together with the regressed estimate based on equation 8.1.*

transport on the sum of the transport in the four shaded sections in figure 3.6 a)

for the whole 98/00 period. The correlation coefficient is 0.87 and the best fit linear estimate for the total transport is

$$\hat{T}_{98/00} = 2.8 \cdot T4_{98/00} - 1.2 \tag{8.1}$$

Although the fields in figure 7.1 are very different, the coefficients in equation 8.1 above do not vary much when the regression is done for 98/99 and 99/00 separately. The values for 98/99 are 2.7 and -1.3, and 2.9 and -1.0 for 99/00. The calculated transport when all instruments are used, and the regression estimate based on four instruments are shown together in figure 8.1 b). Except for two cases the month to month variability in both curves has the same sign, i.e. the regressed transport increases/decreases when the actual transport increases/decreases. Still, the absolute values in individual months may differ with almost one Sv, e.g in January 1999 or March 2000.

An alternative to the above approach could be, as in Ingvaldsen et al. (2002), to make a multivariate regression, i.e. to estimate the transport as $\hat{T}_{98/00} = a \cdot v_{A2} + b \cdot v_{B2} + c \cdot v_{C2} + d \cdot v_{E1} + e$, and then determine five coefficients rather than just two. Since this does not increase the correlations significantly and since the values of the coefficients vary considerably in different time periods (not shown), the simpler method (equation 8.1) has been used in the following.

Figure 8.2 shows the estimated transport based on equation 8.1. With mean value of 3.6 Sv, a monthly mean minimum southward transport of about two Sv (April 1998) and a maximum southward transport of slightly more than five Sv (March 1998), several features of this time series are similar to the 98/00 period. We have to keep in mind that there are large uncertainties in this estimate, but it is interesting to note that also the time of the maximum and the minimum is similar to 98/00. This does at least not contradict the possibility of a seasonal signal.

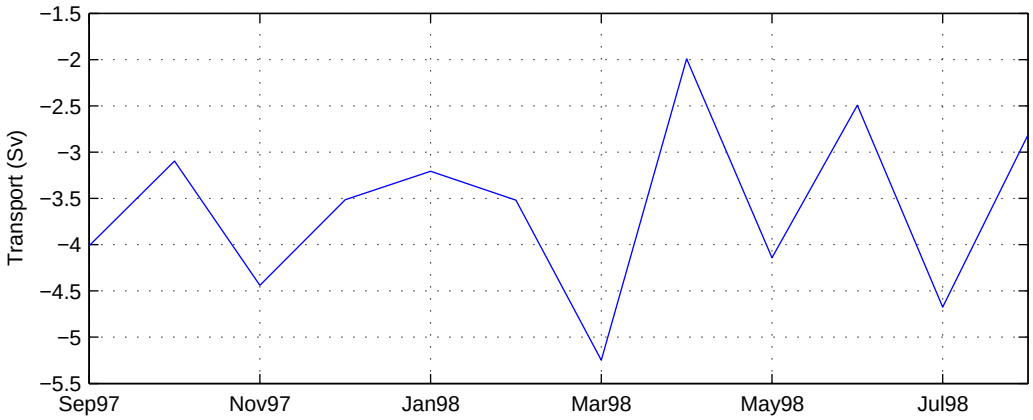

Figure 8.2: *Estimated transport for 97-98 based on equation 8.1.*

To look at the 97/98 period in some more detail, the four time series of cross section velocity used in the transport estimate are shown in figure 8.3. Even if no

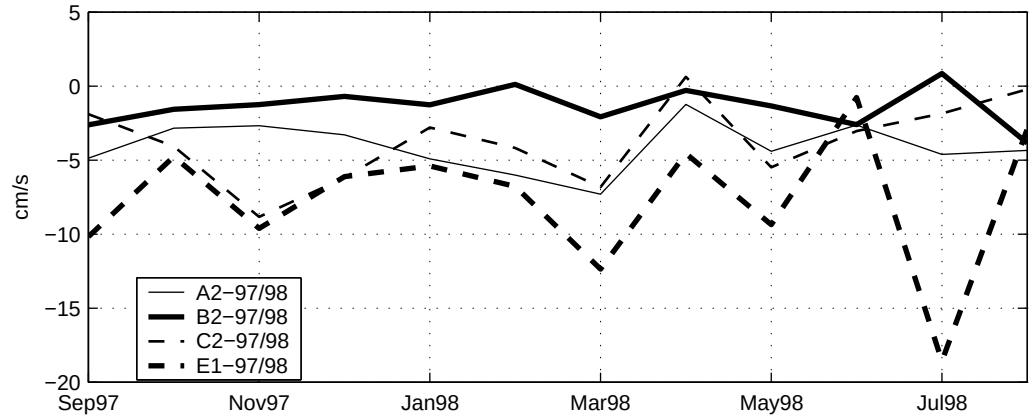

Figure 8.3: *Time series of monthly mean cross section velocity from the four instruments used in the volume transport estimate for 97-98.*

single instrument can be expected to explain the variance in the total volume transport through the section, we may look for some of the features that seemed important in the 98/00 period, e.g. the relatively common occurrences of northward flow at mooring B or the intensifying of the current in the eastern part at the time of maximum transport (figure 4.2, and 6.1).

There were two occurrences of monthly mean northward flow at mooring B in 97/98. In both cases weaker than all such events in 98/00, and it did not happen at the time of estimated minimum southward transport (April 1998). The minimum was instead due to the combined effect of a southward velocity decrease at all instruments. The monthly mean northward flow at mooring C in April 98 was in fact the only case of northward flow at this position throughout the whole 97-00 period. All the instruments also contributed to the maximum southward transport in March 98. The increase was largest in the eastern part, but then again, this instrument was closer to the surface and had overall larger fluctuations. Also note the high southward velocity at mooring E in July 98. This was the overall maximum at this position in the whole 97/00 period.

8.2 Hydrography

Figure 8.4 shows sections of potential temperature and salinity from summer 1997. The amount of PW in the section appears to have been roughly the same as in 1998, i.e. there was more than in 1999, but less than in 2000.

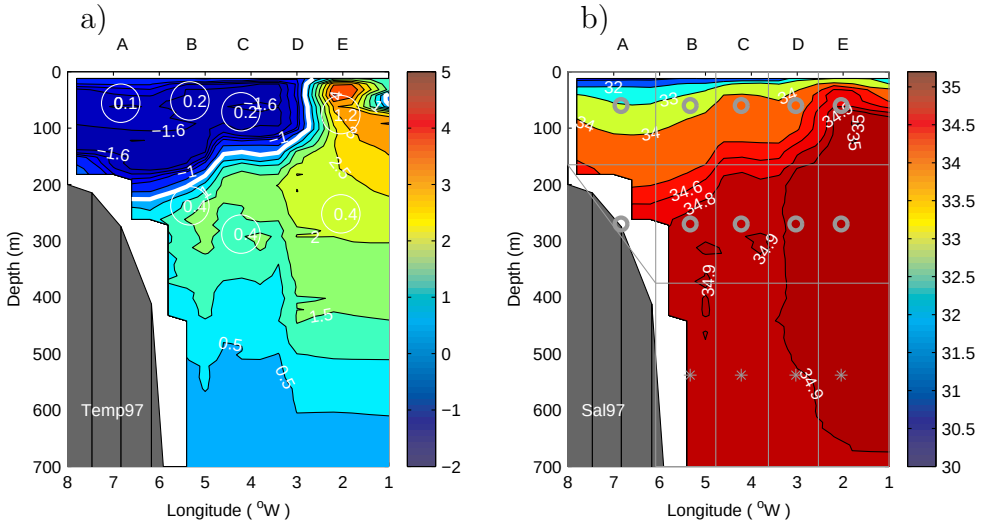

Figure 8.4: *Sections of potential temperature, a), and salinity, b), from summer 1997. Instruments from 97/98 are shown in a). The numbers in the circles are the standard deviation of temperature at the corresponding instrument, based on 6 hour mean values.*

Chapter 9

Mid 80's vs late 90's

9.1 Mean velocity field

Based primarily on the data set in figure 3.6 Foldvik et al. (1988) constructed the mean velocity field shown in figure 9.1 a) for the 84/85 period. Additional information about the surface layer velocities was found from summer drifting buoy data. The eastern boundary for southward flow was set at 1 °W based on the current meters from 1985-1986 (figure 3.6 c), mooring FS9b). Their resulting annual mean transport for 84/85 was 3 Sv.

Due to the sparser data coverage, this estimate cannot readily be compared to the estimate of 3.7 Sv from 98/00. As a first step, rather than to try to estimate an absolute transport, it can be interesting to simply compare mean values of velocity. Figure 9.1 b) shows the mean velocity field from 98/00 as contours (the same as figure 4.1 a)), with the mean values from 84/85 given in the circles.

The area where the difference seems to be largest is in the upper layer around mooring B/FS1. The mean southward velocity in 84/85 was above 6 cm/s while it was between 3 cm/s and 4 cm/s in 98/00. Farther east, around mooring C/FS2 and D/FS3 the differences were smaller.

One possible interpretation of this is suggested by the position of the maximum southward current at the upper instruments. In 84/85 the southward velocity at mooring FS2 was higher than at both mooring FS1 and FS3. In the 98/00 period the maximum southward current in the 60 m level was at mooring D, i.e. farther east. This could indicate that the position of the mean core was farther west in 84/85 than the mean core in 98/00. Figure 9.1 a) shows that this is indeed how Foldvik et al. (1988) interpreted the data. Their velocity maximum is located slightly west of mooring FS3, and the velocity decreases both eastwards and westwards of this, but much more rapidly on the eastern side.

If the velocity field east of mooring FS3 in 84/85 was similar to the 98/00 situation, the 84/85 mooring configuration did not really completely cover the strongest core of

the EGC. This would imply that a transport estimate of 3 Sv for this period probably is too small.

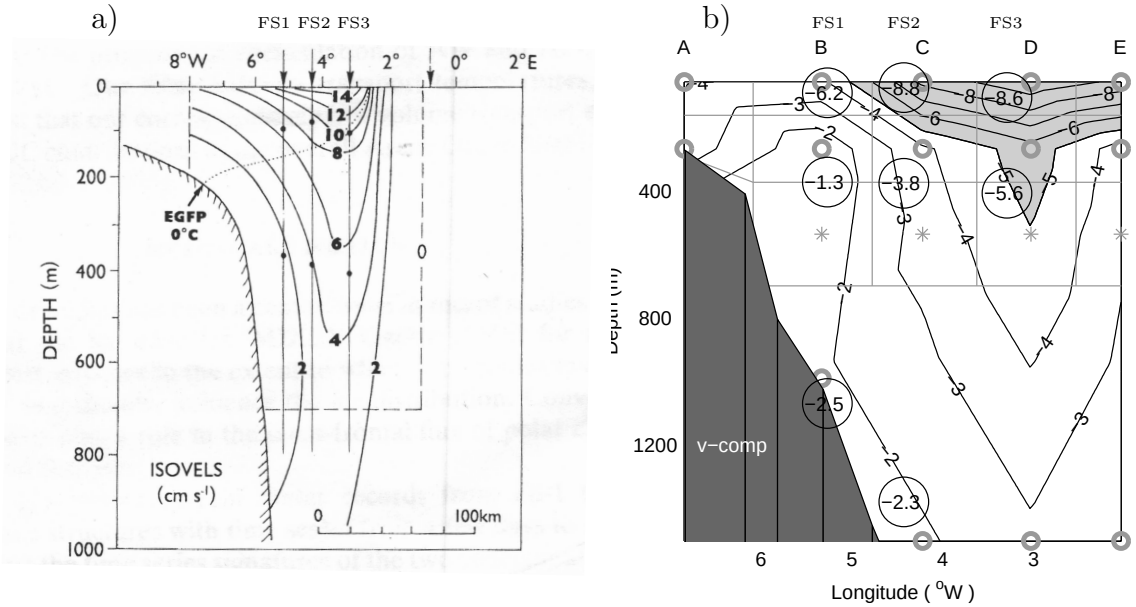

Figure 9.1: *a) constructed annual mean fields of cross section velocity for 84/85 (Taken from Foldvik et al (1988). b) comparison of mean velocities from 98/00 and 84/85. The contours mark the 98/00 field. The circles mark the positions of the instruments from 84/85. The numbers in the circles are the annual mean values of velocity at these positions.*

9.2 Seasonal variability - monthly mean transport

How about the seasonal signal that seems to be present in the late nineties data? From 84/85 we have 6 instruments relatively evenly distributed in the central part of the section and even if an accurate comparison between the transport magnitudes in 84/85 and 98/00 through the whole section is difficult, we may have enough data to look at smaller a part of the section and maybe get some idea of the variability in 84/85 compared to the late 90's. Since there were no instruments in the easternmost and westernmost part of the section in 84/85, we try to estimate the transport through the smaller shaded section in figure 3.6 d). We keep the grid system from the 98/00 estimate and let the upper instruments (FS1-1, FS2-1, FS3-1) represent the uppermost level of sub sections, and the intermediate instruments (FS1-2, FS2-2, FS3-2) represent the two lowermost levels of sub sections. The results are shown in figure 9.2. For comparison the transport through this smaller section for 98/00 period is also shown.

Already from figure 6.1 b) it was evident that the contribution to the total transport from moorings A and E was important in the net transport estimate. This is also confirmed if we compare the total transport from 98/00 (figure 6.1 a)) to the transport

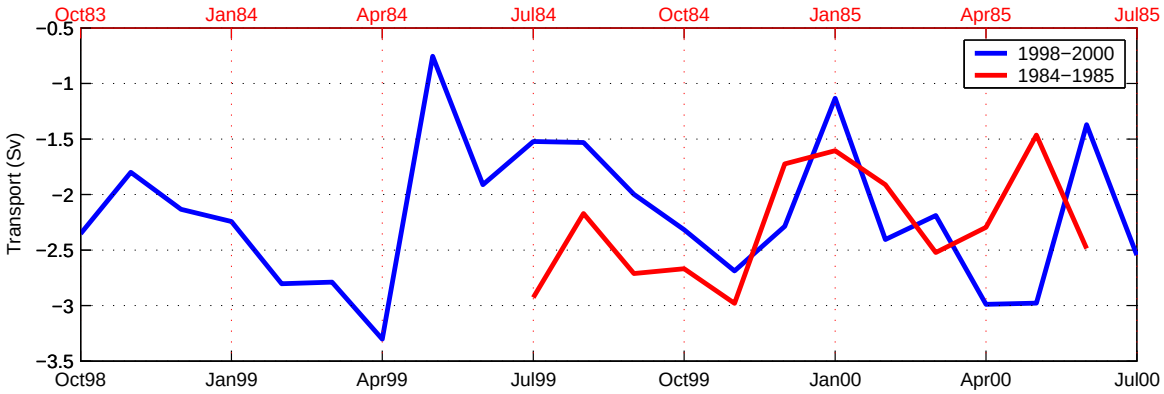

Figure 9.2: *Time series of volume transport from 84/85 (red curve) and98/00 (blue curve) through the shaded section in figure 3.6.*

through the smaller section (figure 9.2, blue curve). The mean transport through the reduced section was 2.2 Sv, i.e. 1.5 Sv less than through the whole section. The late spring / early summer maxima and following minima, of southward transport is present also in this estimate. In addition there seems to be an October maximum that is not present in the full transport estimate.

The mean estimated southward transport for the 84/85 is 2.3 Sv, i.e. essentially equal, when the large uncertainty is taken into consideration. Comparing the periods 84/85, 98/99 and 99/00 it is hard to draw any definite conclusions about the month to month variability and seasonality. 84/85 seems to be qualitatively as similar/different to 98/99 and 99/00 as they are to each other.

9.3 Hydrography

Figure 9.3 shows sections of potential temperature and salinity along 79 °N from summer 1984. Rudels et al. (2000) already pointed out some of the differences between the 1984 sections and the 1997 sections (figure 8.4). Apart from differences in the deep waters (not shown here, see Rudels et al. (2000) figure 3 a) and 16) they also noted that the westward extent of recirculating AW was larger in 1984 than in 1997. This can be seen by comparing the sections of salinity. In 1984 water with salinity of 35 extended almost all the way to the Greenland continental slope. In 1997 there was no water with a salinity of 35 in the section. This was also the case for the other late 90's sections.

Rudels et al. (2000) do not comment differences in the amount of PW (or Polar Surface Water (PSW) using their nomenclature) in the sections. We already noted the strongly varying amount of PW in the CTD sections from the late 90's, both vertically

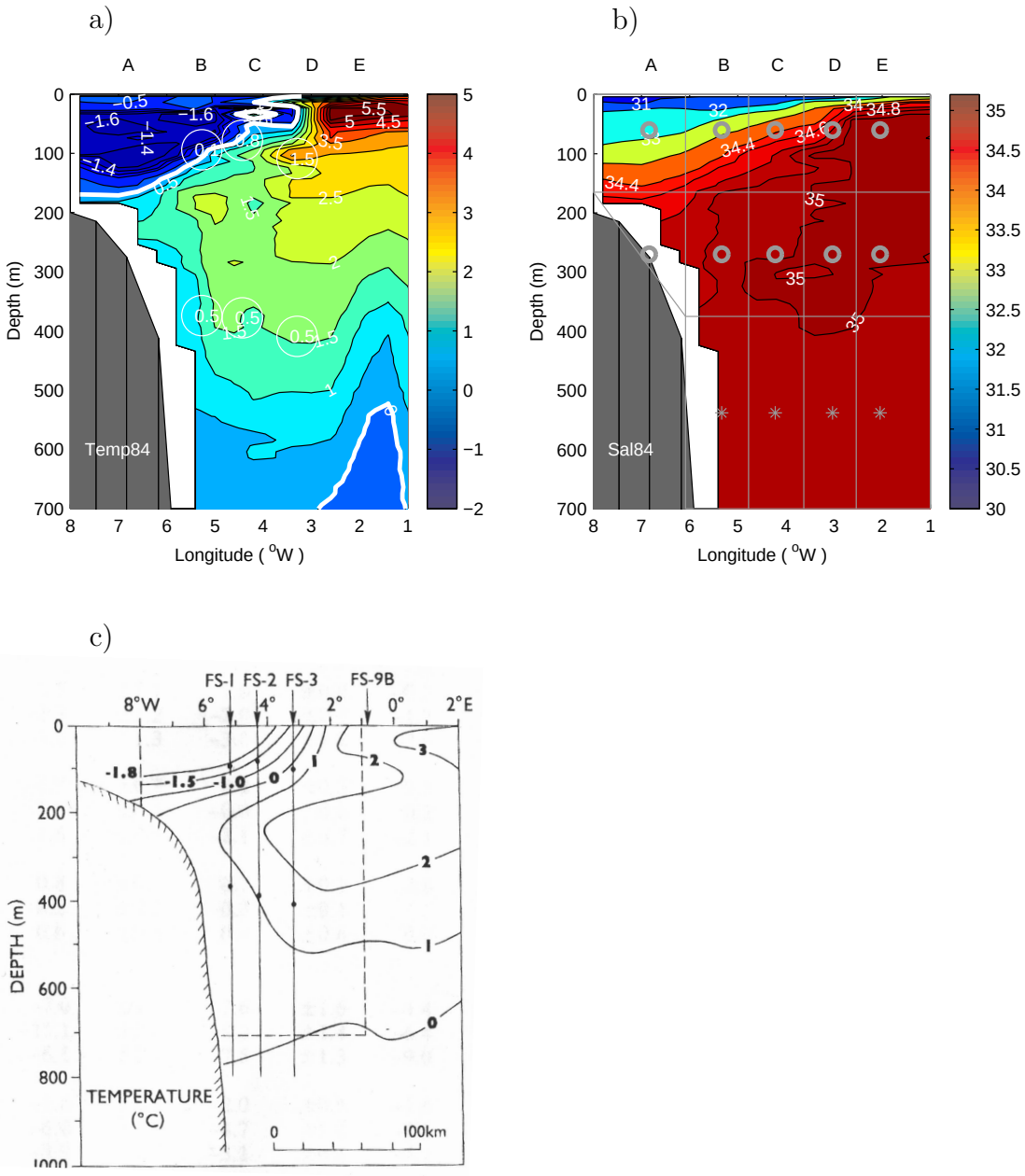

Figure 9.3: *Hydrography 84/85. a) and b) Cross section of potential temperature and salinity from summer 1984 along 79°N, based on ctd measurements. c) Constructed annual mean field of temperature, for the period 1984-1985. Taken from Foldvik et al (1988).*

and horizontally. In summer 84 the extent of PW was less than in all the sections from 1997-2000. If this was representative of the mean situation in the mid 80's, the observed shift in the mean position of the maximum southward current may be related to a shift in the mean position of the Polar Front. Our only sources of information

about the temporal variability of the hydrography are again the temperature sensors mounted on the instruments.

It is probably reasonable to expect larger temperature fluctuations at instruments close to the temperature front. Relatively small variations in the position of the front may cause large temperature changes through advection of a wide range of temperature characteristics past an instrument. A simple measure of variability is given by the standard deviation which thus may provide an indication of how close to the front an individual instrument was. The circles in figure 5.2, figure 8.4 and figure 9.3 show the positions of the instruments that provided temperature data in the period after the CTD stations were occupied. I.e. the instruments from 98/99 are shown in figure 5.2 a), the instruments from 99/00 are shown in figure 5.2 c), the instruments from 97/98 are shown in figure 8.4 a) and the instruments from 84/85 are shown in figure 9.3 a). The numbers in the circles are the standard deviations based on 6 hour mean values of temperature at the corresponding positions and periods.

Let us first consider the 1997-2000 period (figure 8.4, 5.2 a) and c)). The upper instruments at mooring A, B and C have low standard deviations (0.1,0.2) in temperature all years, indicating that these were stably located in PW, away from the front. As we already noted in section 5.1 the upper instruments at mooring D and E were closer to the frontal zone. This is also reflected in the higher standard deviations at these positions.

The positions of the 84/85 instruments were not exactly the same as the positions of the VEINS instruments, but the differences are small enough to allow for a useful comparison. The easternmost and westernmost instruments in the upper level in 84/85 show very similar temperature standard deviations as the instruments at roughly the same positions in the 97-00 period, low (0.1) at mooring FS1 and relatively high (1.5) at mooring FS3. This similarity however is not found between the upper instrument at FS2 and the upper instruments at mooring C from late 90's. The 84/85 standard deviation was 0.8 and in 97-00 the value was 0.2. Figure 9.4 show the time series of temperature from 84/85, 97/98, 98/99 and 99/00 from this position.

The late 90's temperatures (red, yellow and blue curves) were relatively stably low the whole period although all three had a few short periods with peaks of higher temperature values. Most of the time, this was also the case in 84/85. The exception is a period of about one month (August 1984) where temperatures rapidly increased to way above zero, indicating advection of the frontal zone past the instrument. This period is the main reason for for the large standard deviation at this instrument. The CTD data used in figure 9.3 a) and b) were obtained in July/August 1984, i.e. immediately before or in the beginning of the anomalous warm period at FS2-1. Figure 9.3 a) may thus not be very representative of the mean situation in 1984, at least with respect to the amount of PW present in the section. The mean temperature field in figure 9.3 c) from Foldvik et al. (1988) was based on the mean values of temperature

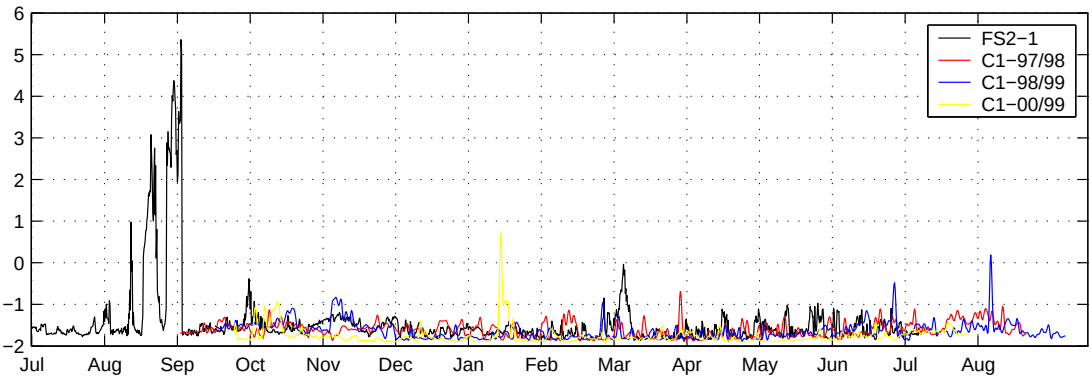

Figure 9.4: *Time series of 6 hour mean values of temperature from the instruments FS2-1 (black curve), C1-97/98 (red curve), C1-98/99 (blue curve) and C1-99/00 (yellow curve). The 84/85 time series started in July while the late 90's time series started in September. The length of all time series is about one year.*

from the moored instruments in addition to various CTD data available at the time. Comparing this to the CTD temperature section from 1984 we see that Foldvik et al. (1988) actually found the mean extent of PW to have been larger than in the 1984 summer situation in the CTD section.

If changes in the position of the polar front was responsible for differences in the mean velocity structures between 84/85 and the late 90's, an extreme temperature anomaly as the one in August/September 1984 (figure 9.4) should somehow show up in the current measurements as well. Figure 9.5 shows the time series of monthly mean velocity from the two uppermost instruments at mooring FS2 and FS3. The highest mean southward velocity was found at the instrument FS2-1 (-8.8 cm/s, figure 9.1). From figure 9.5 a) it is evident that this high value is due to the period from July to September, i.e. roughly the period with the strongest temperature anomalies. Figure 9.5 b) shows the velocities from mooring FS3-1. Here, the same period coincided with minimum southward monthly mean velocity. The time series of temperature from FS3-1 is shown in figure 9.6. Fluctuations around $0°C$ indicate the presence of the front. While most of the year had these frontal characteristics, the period August/September was mainly dominated by warmer water.

The above discussion illustrates the importance of the baroclinic part of the EGC, which due to variability in the position of the Polar Front clearly influences the position of the strongest core of the EGC. There may of course also be other mechanisms involved, but this does at least seem to explain some of the observed differences between 84/85 and the late 90's.

An important point is the consequences this has for estimating the volume transport using reduced data sets (section 7.1). For this approach to work, it is necessary

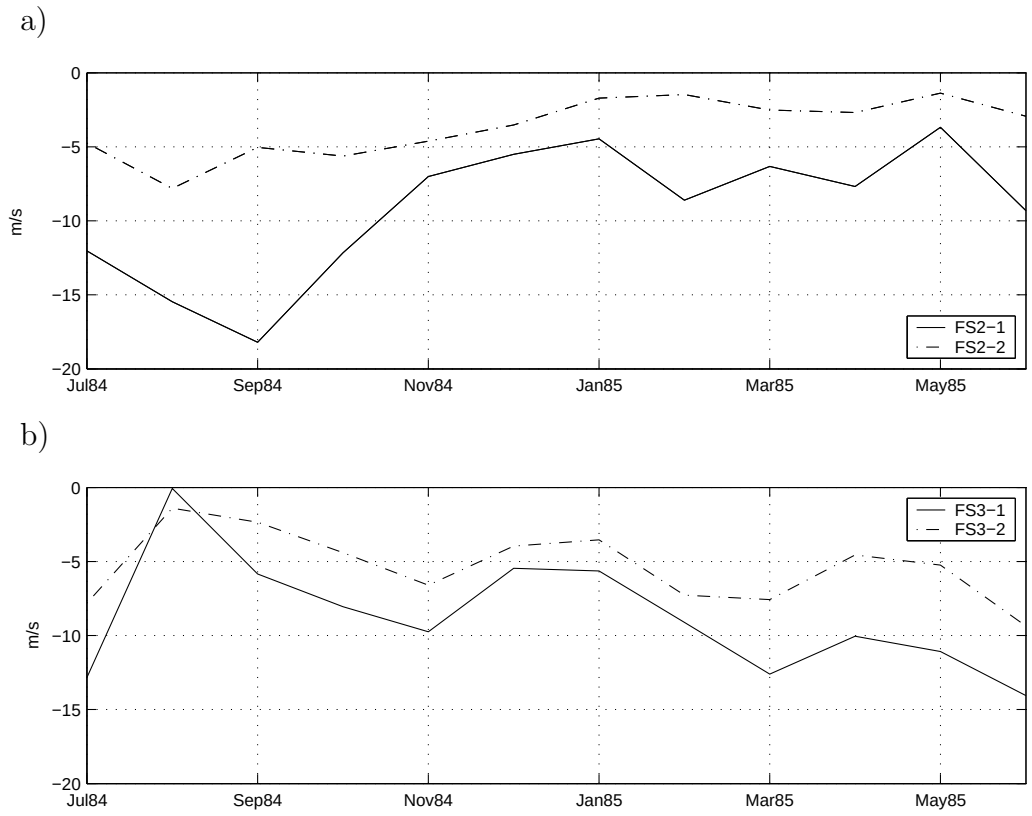

Figure 9.5: *Time series of mean velocity from the two uppermost instruments at moorings FS2 (a)) and FS3 (b)).*

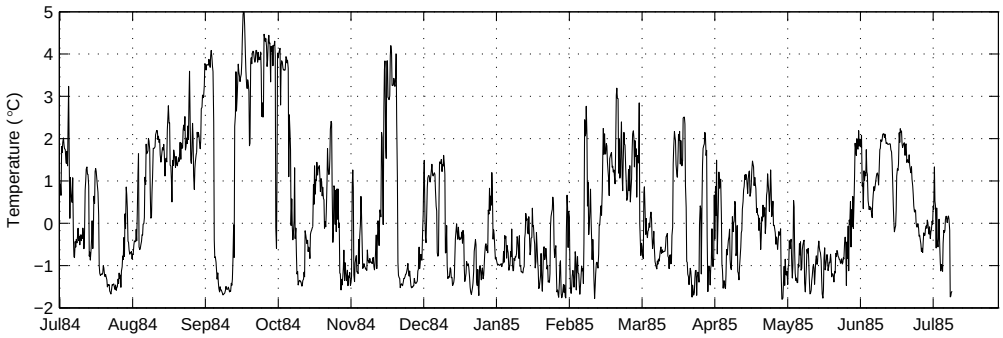

Figure 9.6: *Time series of 6 hour mean values of temperature from FS3-1.*

to assume that the structure in the test period (98/00 in our case) and the estimation period (e.g. 84/85) are fairly similar. Due to the differences discussed above, this assumption is not necessarily valid in the EGC.

It is not obvious that the mean position of the Polar front has moved eastward

from the mid 80's to the late 90's. However, at least there were periods in 1984 where the front was much farther west than in the whole period from 1997-2000. This and the fact that all summer CTD sections from the late 90's had a larger PW extent than the summer section from 84 does at least not contradict the possibility that there has been a change. This would probably imply a different freshwater transport in the EGC. Foldvik et al. (1988) calculated a mean transport of PW ($T < 0°C$) for 84/85 of 1 Sv. Aagard and Carmack (1989) argued that relative to a reference salinity of 34.93 the transport of PW is by far the largest contribution to the liquid freshwater export to the Greenland Sea through the Fram Strait. They estimated a mean PW salinity of 33.7. This yields a freshwater transport of 1110 km^3yr^{-1}. Correspondingly, if we assume the same PW salinity, our PW transport estimate of 1.4 Sv yields a 40 % larger freshwater transport, i.e. 1554 km^3yr^{-1}, which does support the possibility of increased freshwater transport. The errors in these estimates are however very large.

Chapter 10

Further discussion

10.1 Mesoscale variability

So far we have mainly focused on net north-south transports and variability on annual and monthly time scales. The EOF analysis in section 7.2 indicates that a large fraction of the variability in the EGC does not directly contribute to the net transport across 79 ° N. Based on the 1984-1985 data set shown in figure 3.6, Foldvik et al. (1988) noted the abundance of eddy-like structures with time scales from a few days to several weeks in the area between mooring B and mooring D. This is one possible source of the variability in the first EOF mode (section 7.2). A thorough study of the mesoscale activity is beyond the scope of this work, but to at least show one example of this from the 98-00 data set, a stick plot of full record length, 6 hour mean, low pass filtered velocities from D2-99/00 is shown in figure 10.1. This instrument was located close to what seems to be the core of the mean current, in an area with annual mean southward velocity of about 6 cm/s (figure 4.1 a)). Clearly the strong month to month variability is a result of even more extreme fluctuations on much shorter time scales. As an example consider January 2000, the most anomalous month in figure 4.2. There were roughly 4 periods of between 4 to 10 days length, with a northward current component. In between these there were periods of southward current. In both directions, speeds got close to 20 cm/s. Although this was the only month with a monthly mean northward velocity at this position, northward velocities and sudden changes in speed and direction was a relatively common feature throughout the whole period. Foldvik et al. (1988) suggests that the advection of eddies past the instrument would produce signatures similar to the ones observed in the EGC. The details will of course depend on the relative strength of the eddies, the velocity distribution within the eddies, and the ambient velocity field. Still, clockwise rotating eddies will produce diverging stick diagrams (e.g like around the 13'th of January) and counter clockwise rotating eddies will produce converging stick diagrams (e.g like around the 17'th of February).

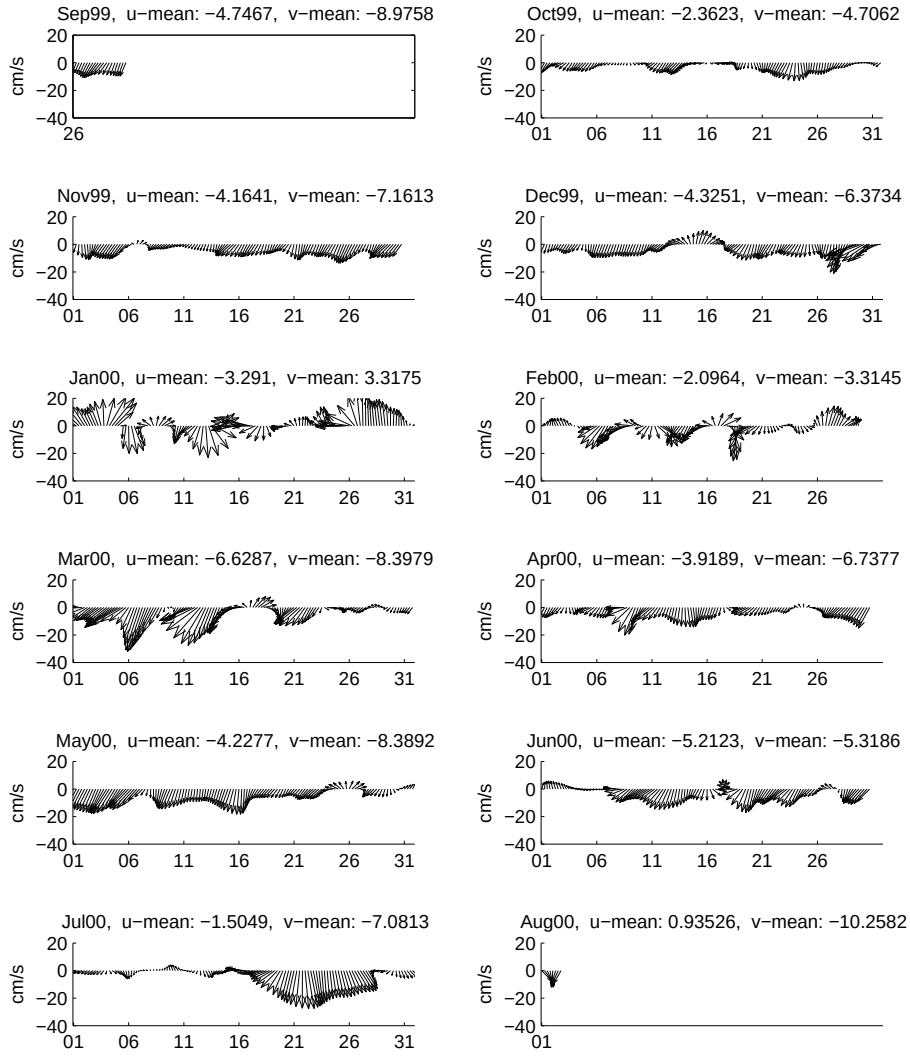

Figure 10.1: *Stickplot of 6-hour mean, low-passed velocity from D2-99/00. Monthly mean values are given above each figure. The scaling is given in the y-axis.*

Various sources of the mesocale activity in the area have been proposed (see Jonsson et al. (1992) for a short review). E.g. Johannessen et al. (1987) suggest various types of instabilities as the source of eddies while Gascard et al. (1988) suggest that the EGC is dynamically stable and that eddies are advected from the east rather than generated through instabilities. The role of wind forcing in the generation of the mesoscale variability in the Fram strait have been discussed by e.g Jonsson et al. (1992). They found that most of the observed eddy kinetic energy in at least the central and eastern Fram Strait was generated by wind fluctuations, rather than through flow instabilities. They were however not conclusive about the origin of the mesoscale variability in the EGC.

10.2 Water masses

Much of the variability in the monthly mean velocity fields is probably related to the large mesoscale activity in the area (section 10.1). The time series of temperature in figure 5.1 show changes that seem to reflect long term variability, especially in the intermediate (270 m) level. The colder water in the western part is as we already noted probably due to increased vertical extent of the PW. If we again use standard deviations as an indicator of the distance to the front, and compare the values from the instruments B2-97/98 (figure 8.4 a)), B2-98/99 (figure 5.2 a)) and B2-99/00 (figure 5.2 c)), they also indicate that the front was deeper in 99/00 than in 97/98 and 98/99. The values are 0.4, 0.5 and 1.0 for 97/98, 98/99 and 99/00 respectively.

The observations of warmer water in the eastern part from summer 1999 onwards may have several explanations. First of all, the extreme January 2000 situation is probably related to the anomalous flow field (figure 4.2 and 10.1). A monthly mean temperature above 3 $^{\circ}C$ (i.e. AW) indicates an extreme case of WSC influence. A stronger recirculation, or a warmer recirculation may of course also be responsible for the observed changes in the rest of the period. Another possibility also exists. Remnants of the observed warming of the Atlantic layer in the Arctic Ocean is expected to exit through the Fram Strait (Gerdes et al. 2003). Combinations of these scenarios are of course also possible.

10.3 Forcing

E.g. Widell et al. (2003) and Vinje et al. (1998) have found high correlations between atmospheric pressure differences (i.e. wind forcing) and the ice transport through the Fram Strait. It is also interesting to compare the variability in the EGC to the same pressure differences.

The effects of direct wind forcing on ocean dynamics is not as straight forward as on ice drift. The influence of wind (or ice) through the drag on the water surface is limited to the relatively shallow Ekman surface layer. Pond and Pickard (1983) gives a value of about 45 m depth for a wind speed of 10 m/s at 80°N. Still, this upper layer influence may in turn effect the geostrophic balance through the entire water column. This is due to surface elevations and the barotropic currents that may result from the transport induced by the wind forcing. The net wind induced transport in the Ekman layer is, due to the earth's rotation, directed 90° to the right (northern hemisphere) of the direction of the forcing on the surface. An east-west pressure difference in the Fram Strait would for instance produce geostrophic winds across the section (north-south). They may in turn lead to east-west surface elevations and thus north-south

geostrophic currents. A north-south pressure difference would in the same manner create north-south ekman transports in the surface layer.

E.g. Ingvaldsen et al. (2004b) found this mechanism to be an important controlling factor in the inflow to the Barents Sea.

Vinje et al. (1998) used the pressure difference between $81°N10°W$ and $73°N20°E$. Widell et al. (2003) tested many possibilities and ended up using the local pressure difference right across the outflow, between 80°N15°W and 80°N5°W to estimate ice transport. Figure 10.2 shows the volume transport for the 98/00 period (black curve), together with the east-west pressure difference used by Widell et al. (2003) (red curve), and a north-south pressure difference between 80°N2.5°W and 77.5°N2.5°W (red dotted curve).

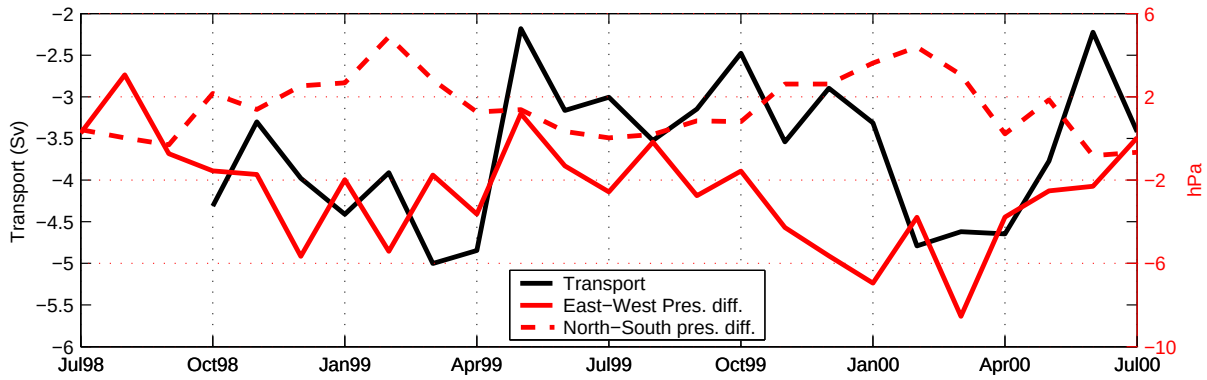

Figure 10.2: *Comparison of the volume transport in the EGC to the local atmospheric forcing. The black curve shows the total transport, the full red line shows the surface pressure difference between 80° N15° W and 80° N5° W and the red dotted line shows the surface pressure difference between 80° N2.5° W and 77.5° N2.5° W. The pressure differences are calculated from NCEP/NCAR data.*

A visual inspection shows little resemblance between the variability in the pressure differences and the variability in the volume transport. The correlations between the volume transport and both of the pressure differences are highest when calculated with some time lag, i.e. when the wind precedes the transport with a few months. The correlation between the north-south pressure difference and the transport two months later is $r = 0.5$. One month delay gives a maximum value of 0.4 for the east-west pressure difference.

These are anyway low values, the local wind forcing does not explain much of the monthly variability in the net transport. However, there is a strong seasonal signal in the wind forcing in the area (Jonsson et al. 1992). This is also evident from figure 10.2. The pressure differences are largest in winter, i.e prior to the observed maxima of southward transport in the EGC. It is possible that wind forcing may explain part of the seasonal signal in the transport, but that it in periods of weaker forcing becomes less important.

Orvik and Skagseth (2003b) found a high correlation (0.88) between the wind stress curl in the North Atlantic and the transport in the NwASC 15 months later. In our case only a 22 month long continuous time series is available. This is not sufficient for studying such time lags. The monitoring of the Fram Strait has continued as a part of the Arctic/Subarctic Ocean Fluxes (ASOF) program. This will enable the construction of longer time series and thus the possibility to search for connections to larger scale features.

There is however one fundamental difference between these areas, the complexity in the composition of water masses. The fact that the EGC in the Fram Strait is a composite of water from very different sources converging in the strait, probably makes it difficult to find one forcing mechanism that explains all the variability. There are at least three distinct water masses only in the upper layers of the EGC: the PW, the intermediate waters exiting the Arctic Ocean and the Atlantic water recirculating in the strait. Better results may possibly be obtained by studying these separately.

Consider for instance the recirculation of Atlantic water. This is probably somehow related to the variability in the WSC. Fahrbach et al. (2001) found a strong seasonal cycle in the WSC, with maximum northward transport in winter (February) and minimum in summer (August). This is similar to our observed transport variability in the EGC. If increased transport in the WSC leads to increased recirculation this may thus explain some of the seasonal signal in the EGC. Also, if the WSC is more directly forced by local winds than the EGC, the time lag in correlations between EGC transport and pressure differences may be related to the time it takes for the recirculating WSC signal to cross the strait.

Chapter 11

Summary and conclusions

The Fram Strait is in many respects an ideal site for climate monitoring in the sense that much of the variability in the Arctic Ocean / Nordic Seas should somehow show up in measurements from this area. The initial intention of this work was to investigate the possibility of constructing longer time series of variability in the upper and intermediate layers of the EGC in the Fram Strait. This is not straightforward since both the temporal and the spatial instrument coverage varied considerably in the study period, 1984-2000. The most extensive set of current measurements was collected as a part of the VEINS program from 1998 to 2000. This data set was first used to provide a fairly detailed picture of the 1998-2000 period, and then as a basis for comparison to other periods.

Some of the main conclusions are listed below:

- **1998-2000 - Volume transport**
  The mean southward transport of upper and intermediate water in the EGC was estimated to 3.7 Sv. Of this 1.4 Sv was PW and 2.3 Sv was AIW. In the 98/99 the total transport was slightly higher (3.8 Sv) and in 99/00 slightly lower (3.5 Sv). Both years had maximum transport in late winter / early spring followed by transport minima shortly after, in late spring / early summer

- **Possibilities of constructing longer time series of volume transport**

  The linear relationship between variability of velocity from individual instruments and total volume transport was tested by correlation for the 1998-2000 period. No instruments describe the transport variability well enough to make reliable regression estimates. With our present understanding of the governing mechanisms of variability in the EGC, construction of transport estimates for large parts of the 1984-1998 period seems difficult.

- **1997-1998**
  Sparser data coverage makes uncertainties in volume transport for this period

larger. Still, a simple regression estimate based on velocity from four instruments gave the same mean transport and roughly the same seasonal signal as in the 1998-2000 period.

- **Mid 80's vs late 90's**
  The structure of the mean velocity field differed slightly in the two periods. Comparisons of velocity measurements and temperature measurements show that this was largely due to strong fluctuations in the position of the Polar Front in the late summer / early autumn of 1984. These structural differences may however not necessarily imply that the net volume transport across the section was very different. The 84/85 data set covers the central part of the section fairly well. A comparison of transports through a slightly reduced section show no significant differences between the 84/85 and the 98/00 periods.

- **Forcing**
  The forcing mechanisms of the EGC are complex and not very well understood. Here, the importance of the local atmospheric pressure field (i.e. winds) on the monthly mean transport was tested through correlation. Although possibly important for periods with strong winds, most of the month to month transport variability cannot be explained by local atmospheric pressure differences. To understand the forcing of the EGC it is probably necessary to understand the forcing of the various source waters. Part of the seasonal signal in the EGC may e.g. be related to the forcing of the WSC through recirculation.

Appendix A

EOF analysis

Empirical Orthogonal Functions (EOF) analysis is described by e.g. Emery and Thomson (2001). There are two ways of calculating the EOF's in section 7.2, namely through an eigenvalue analysis of the covariance matrix, or through Singular Value Decomposition (SVD). The methods produce the same results. Here the first method is presented.

If we organize our 14 time series, each with 22 monthly mean values of velocity, into a two dimensional 22 x 14 matrix V, and remove the mean from each column (i.e. from each time series), the covariance matrix R of V is given by $R = V^tV$. Here V^t denotes the transpose of V. It can be shown that the desire to explain as much of the variance in the data set as possible, with the fewest possible standing oscillations, corresponds to an eigenvalue analysis of the covariance matrix:

$$RE = LE \tag{A.1}$$

Here E is the matrix with the eigenvectors e_i as its columns and L is the matrix with the eigenvalues along its diagonal. All the other elements in L are zero. Each eigenvector is one EOF. The EOF that explains most of the variability, the first mode, is the eigenvector e_1 associated with the largest eigenvalue. The fraction of the variance explained by the mode associated with an eigenvalue, is found by dividing the particular eigenvalue by the sum of all the eigenvalues. In our case the eigenvectors e_i (the EOF's) have 14 elements, one element associated with each of the 14 instruments. The pattern obtained when an EOF is plotted as a contour field (as in figure 7.2 a) and b)) represents a visualization of a standing oscillation.

The time variability of e.g. EOF1 is found from:

$$\overrightarrow{pc_1} = V\overrightarrow{e_1} \tag{A.2}$$

where $\overrightarrow{pc_1}$ is the principal component (PC) time series. In our case the PC's have 22 elements, i.e. the same as the length of the time series. The first two PC's are shown in figure 7.2 c) and d).

References

Aagaard, K. (1989). A synthesis of the Arctic Ocean circulation. *Rapp.P.V. Reun. Cons. Int. Explor. Mer. 188*, 11–22.

Aagaard, K., C. Darnall, A. Foldvik, M. Steg, and T. Tørresen (1988). Fram Strait current measurements 1985-1986. *Univ of Bergen, Norway, Rep. 66*.

Aagaard, K., C. Darnall, A. Foldvik, and T. Tørresen (1985). Fram Strait current measurements 1984-1985. *Univ. of Bergen, Norway, Rep. 63*.

Aagaard, K., A. Foldvik, and S. R. Hillman (1987). The West Spitsbergen Current: Disposition and Water Mass Transformation. *Journal of Geophysical Research 92*(C4).

Aagard, K. and E. C. Carmack (1989). The Role of Sea Ice and Other Fresh Water in the Arctic Circulation. *Journal of Geophysical Research 94*(C10), 14,485–14,498.

Carmack, E. C. (2000). *The Arctic Ocean's freshwater budget: Sources, storage and export*, Chapter 4, pp. 91–126. NATO Science Series 2(70), Kluwer Academic Publishers, Dordrecht.

Carmack, E. C., R. W. Macdonald, R. G. Perkin, F. A. McLaughlin, and R. J. Pearson (1995). Evidence for warming of Atlantic water in the southern Canadian Basin of the Arctic Ocean: Results from the Larsen-93 expedition. *Geophysical Research Letters 22*(9), 1061–1064.

Dickson, B. (1999). All change in the Arctic. *Nature 397*.

Emery, W. J. and R. E. Thomson (2001). *Data analysis Methods in Physical Oceanography* (2nd ed.). Elsevier Science B.V.

Fahrbach, E. (1999). The Expedition ARK XIV/2 of the Research Vessel Polarstern in 1998. *Rep. Polar Res., Alfred-Wegener-Inst., Bremehaven, Germany 326*.

Fahrbach, E., J. Meinche, S. Østerhus, G. Rohardt, U. Schauer, V. Tverberg, and J. Verduin (2001). Direct measurements of volume transports through Fram Strait. *Polar Research 20*(2), 217–224.

Foldvik, A., K. Aagaard, and T. Tørresen (1988). On the velocity field of the East Greenland Current. *Deep-Sea Research 35*(8), 1335–1354.

Friedrich, H., M. N. Houssais, D. Quadfasel, and B. Rudels (1995). On Fram Strait Water Masses. *Extended Abstract, Nordic Seas Symposium, Hamburg 7/3-9/3*, 69–72.

Gascard, J. C., C. Kergomard, P. F. Jeannin, and M. Fily (1988). Diagnostic study of the Fram Strait marginal ice zone during summer from 1983 and 1984 Marginal Ice Zone experiment Lagrangian observations. *Journal of Geophysical Research 93*(C4), 3613–3641.

Gerdes, R., M. Karcher, F. Kauker, and U. Schauer (2003). Causes and development of repeated Arctic Ocean Warming events. *Geophysical Research Letters 30*(19).

Grotefendt, K., K. Logemann, D. Quadfasel, and S. Ronski (1998). Is the Arctic Ocean warming? *Journal of Geophysical Research 103*(C12), 27,679–27,687.

Hansen, B. and S. Østerhus (2000). North Atlantic-Nordic Seas exchanges. *Progress in Oceanography 45*, 109–208.

Ingvaldsen, R., L. Asplin, and H. Loeng (2004a). The seasonal cycle in the Atlantic transport to the Barents Sea during the years 1997-2001. *Continental Shelf Research 24*, 1015–1032.

Ingvaldsen, R., L. Asplin, and H. Loeng (2004b). Velocity field of the western entrance to the Barents Sea. *Journal of Geophysical Research 109*.

Ingvaldsen, R., H. Loeng, and L. Asplin (2002). Variability in the Atlantic inflow to the Barents Sea based on a one-year time series from moored current meters. *Continental Shelf Research 22*, 505–519.

Johannessen, J. A., O. M. Johannessen, E. Svendsen, R. Schucman, T. Manley, W. J. Campbell, E. G. Josberger, S. Sandven, J. C. Gascard, T. Olaussen, K. Davidson, and J. Vanleer (1987). Mesoscale eddies in the Fram Strait marginal ice zone during the 1983 and 1984 Marginal Ice Zone Experiments. *Journal of Geophysical Research 92*(C7), 6754–6772.

Johannessen, O. M., E. V. Shalina, and M. W. Miles (1999). Satelite Evidence for an Arctic Sea Ice Cover in Transformation. *Science 286*.

Jonsson, S., A. Foldvik, and K. Aagaard (1992). The structure and Atmospheric forcing of the Mesoscale Velocity Field in Fram Strait. *Journal of Geophysical Research 97*(C8), 12585–12600.

Kasajima, Y. and H. Svendsen (2002). Tidal features in the Fram Strait. *Continental Shelf Research 22*, 2461–2477.

Meinche, J., B. Rudels, and H. J. Friedrich (1997). The Arctic Ocean-Nordic Seas thermohaline system. *ICES Journal of Marine Science 54*, 283–299.

Orvik, K. A. and P. Niiler (2002). Major pathways of Atlantic water in the northern North Atlantic and Nordic Seas toward Arctic. *Geophysical Research Letters 29*(19).

Orvik, K. A. and O. Skagseth (2003a). Monitoring the Norwegian Atlantic slope current using a single moored current meter. *Continental Shelf Research 23*, 159–176.

Orvik, K. A. and O. Skagseth (2003b). The impact of the wind stress curl in the North Atlantic on the Atlantic inflow to the Norwegian Sea toward the Arctic. *Geophysical Research Letters 30(17)*.

Pond, S. and G. L. Pickard (1983). *Introductory Dynamical Oceanography* (2nd ed.). Butterworth-Heinemann.

Rothrock, D. A., Y. Yu, and G. A. Maykut (1999). Thinning of the Arctic Sea-ice Cover. *Geophysical Research Letters 26*(23), 3469–3472.

Rudels, B., E. Fahrbach, J. Meinche, G. Budeus, and P. Eriksson (2002). The East Greenland Current and its contribution to the Denmark Strait overflow. *ICES Journal of Marine Science 59*, 1133–1154.

Rudels, B., R. Meyer, E. Fahrbach, V. V. Ivanov, S. Østerhus, D. Quadfasel, U. Schauer, V. Tverberg, and R. A. Woodgate (2000). Water mass distribution in Fram Strait and over the Yermak Plateau in summer 1997. *Ann. Geophysicae 18*, 687–705.

Schauer, U. (2000). The Expedition ARK XV/3 of the Research Vessel Polarstern in 1999. *Rep. Polar Res., Alfred-Wegener-Inst., Bremehaven, Germany 350*.

Schauer, U., E. Fahrbach, S. Østerhus, and G. Rohardt (2004). Arctic warming through the Fram Strait: Oceanic heat transport from 3 years of measurements. *Journal of Geophysical Research 109*.

Schlosser, P., G. Bönisch, M. Rhein, and R. Bayer (1991). Reduction of Deepwater Formation in the Greenland Sea During the 1980s: Evidence from Tracer Data. *Science 251*.

Simonsen, K. and P. M. Haugan (1996). Heat budgets of the Arctic Mediterranean and sea surface heat flux parameterizations for the Nordic Seas. *Journal of Geophysical Research 101*(C3), 6533–6576.

Steele, M. and T. Boyd (1998). Retreat of the cold halocline layer in the Arctic Ocean. *Journal of Geophysical Research 103*(55), 10,419–10,435.

Østerhus, S. and T. Gammelsrød (1999). The Abyss of the Nordic Seas is warming. *Journal of Climate 12*(11).

Swift, J. H. and K. Aagaard (1981). Seasonal transitions and water mass formation in the Iceland and Greenland seas. *Deep-Sea Research 28A*(10), 1107–1129.

Vinje, T. (2001). Fram Strait Ice Fluxes and Atmospheric Circulation: 1950-2000. *Journal of Climate 14*.

Vinje, T., N. Nordlund, and A. Kvambekk (1998). Monitoring ice thickness in Fram Strait. *Journal of Geophysical Research 103*(C5), 10,437–10,449.

Widell, K., S. Østerhus, and T. Gammelsrød (2003). Sea ice velocity in the Fram Strait monitored by moored instruments. *Geophysical Research Letters 30*(19).

Woodgate, R., U. Schauer, and E. Fahrbach (1998). Moored current meters in the Fram Strait at 79N: Preliminary results with special emphasis on the West Spitsbergen Current. *Ber. Fachber. Phys., Alfred-Wegener-Inst., Bremehaven, Germany 91*.

Woodgate, R. A., E. Fahrbach, and G. Rohardt (1999). Structure and transport of the East Greenland Current at 75° N from moored current meters. *Journal of Geophysical Research 104*(C8), 18059–18072.